Distribution Agreement

In presenting this thesis as a partial fulfillment of the requirements for a degree from Emory University, I hereby grant to Emory University and its agents the non-exclusive license to archive, make accessible, and display my thesis in whole or in part in all forms of media, now or hereafter now, including display on the World Wide Web. I understand that I may select some access restrictions as part of the online submission of this thesis. I retain all ownership rights to the copyright of the thesis. I also retain the right to use in future works (such as articles or books) all or part of this thesis.

Hannah Kelly March 24, 2019

Ultrastructural Plasticity of Pallidothalamic GABAergic Terminals in Parkinson's Disease: A 3D Electron Microscopy Study in the Parvocellular Ventral Anterior and Centromedian Thalamic Nuclei in MPTP-Treated Parkinsonian Monkeys

by

Hannah Kelly

Yoland Smith, Ph.D.
Adviser

Neuroscience and Behavioral Biology

Yoland Smith, Ph.D.

Adviser

Rosa Villalba, Ph.D.

Committee Member

Leah Roesch, Ph.D.

Committee Member

2019

Ultrastructural Plasticity of Pallidothalamic GABAergic Terminals in Parkinson's Disease: A 3D Electron Microscopy Study in the Parvocellular Ventral Anterior and Centromedian Thalamic Nuclei in MPTP-Treated Parkinsonian Monkeys

By

Hannah Kelly

Yoland Smith, Ph.D.

Adviser

An abstract of
a thesis submitted to the Faculty of Emory College of Arts and Sciences
of Emory University in partial fulfillment
of the requirements of the degree of
Bachelor of Sciences with Honors

Neuroscience and Behavioral Biology

2019

Abstract

Ultrastructural Plasticity of Pallidothalamic GABAergic Terminals in Parkinson's Disease: A 3D Electron Microscopy Study in the Parvocellular Ventral Anterior and Centromedian Thalamic Nuclei in MPTP-Treated Parkinsonian Monkeys

By Hannah Kelly

The internal globus pallidus (GPi) is the main source of basal ganglia GABAergic afferents to the parvocellular region of the ventral anterior nucleus (VApc) and the centromedian nucleus (CM) in the thalamus. Models of the basal ganglia-thalamocortical circuitry predict that nigrostriatal dopamine loss causes abnormally increased GABAergic pallidal outflow to the thalamus in Parkinson's disease (PD). However, our understanding of the pathophysiology and underlying anatomical substrates of this increased pallidothalamic activity remains limited. Electrophysiological studies have reported complex changes in firing rates of thalamocortical neurons in animal models of parkinsonism and in PD patients. In the striatum and subthalamic nucleus, altered neuronal activity in the parkinsonian state is associated with structural changes in GABAergic and glutamatergic synapses. The GPi gives rise to large GABAergic terminals forming multiple axo-dendritic synapses in the VApc and CM. Functional data gathered from structurally-similar terminals in other regions suggests that the multi-synaptic morphology of GPi-like terminals creates favorable conditions for inter-synaptic spillover of GABA, which may enable tonic inhibition even under conditions of high presynaptic firing rates.

Understanding ultrastructural changes of pallidothalamic terminals will help elucidate the impact of altered GPi outflow onto thalamocortical neurons in parkinsonism. To address this, we used serial block-face scanning electron microscopy to quantitatively compare the morphology of GPi terminals in the VApc and CM of control and MPTP-treated parkinsonian monkeys. Preliminary results suggest that the following structural changes take place in parkinsonian animals: the volume of GPi terminals is enlarged in VApc and CM; the average number of synapses per terminal is decreased in VApc and increased in CM; and the surface areas of synapses formed by terminals are increased in VApc and CM. These findings indicate that pallidothalamic terminals are endowed with a high level of structural plasticity possibly contributing to increased tonic regulation of thalamocortical outflow in PD. Our data also demonstrate target-specific differences in the ultrastructure of GPi terminals that innervate VApc vs. CM neurons, which may underlie physiological differences in the effects of pallidal output to these thalamic targets.

Ultrastructural Plasticity of Pallidothalamic GABAergic Terminals in Parkinson's Disease: A 3D Electron Microscopy Study in the Parvocellular Ventral Anterior and Centromedian Thalamic Nuclei in MPTP-Treated Parkinsonian Monkeys

By

Hannah Kelly

Yoland Smith, Ph.D.

Adviser

A thesis submitted to the Faculty of Emory College of Arts and Sciences
of Emory University in partial fulfillment
of the requirements of the degree of
Bachelor of Sciences with Honors

Neuroscience and Behavioral Biology

2019

Acknowledgements

First, I would like to express my gratitude to my adviser, Dr. Yoland Smith. I couldn't have asked for a more knowledgeable and supportive mentor, and I can't thank him enough for the outstanding scientific training he has provided. I am sincerely grateful for the potential he saw in me and for his unwavering guidance and dedication to my achievement. I also want to thank my other committee members, Dr. Rosa Villalba and Dr. Leah Roesch. I truly appreciate their continuous support throughout this process and for contributing to my success by providing constant advice and encouragement. Thank you to my lab colleagues—Susan Jenkins, Jeff Paré, and Gunasingh Jeyaraj—for making the lab such a welcoming and friendly environment to work in over the past three years. Finally, I owe a huge thank you to Dr. Ashley Swain for being a wonderful role model. I am truly grateful she took me under her wing three years ago and trusted me to assist in collecting data for her dissertation. Her mentorship and the independence she instilled in me have been more valuable than I could have imagined. Thank you to all of the above people and to my family and friends for your continuous love and support throughout my journey at Emory.

Table of Contents

List of Figures and Tables

Introduction

Background

Affecting 60,000 new patients each year in the United States, Parkinson's disease (PD) is the second most prevalent neurodegenerative disease. Parkinson's disease is associated with extensive degeneration of the dopaminergic nigrostriatal system of the basal ganglia, which causes the cardinal motor symptoms of PD—resting tremor, bradykinesia, rigidity, and akinesia. Despite considerable advances in understanding the anatomy and functioning of the basal ganglia throughout the past decades, our current knowledge of processing of information in the basal ganglia-thalamocortical loop remains incomplete. A more comprehensive understanding of the functional anatomy and synaptic connectivity of this circuitry in both normal and diseased states is necessary to elucidate network changes potentially contributing to aspects of Parkinson's disease pathophysiology.

General Organization of the Basal Ganglia

Several intertwined subcortical structures consisting of the caudate nucleus and putamen (the striatum), the internal and external segments of the globus pallidus (GPe and GPi), the substantia nigra (SN), and the subthalamic nucleus (STN) constitute the basal ganglia (Wichmann and DeLong, 1996). Cortical information enters the basal ganglia via topographic, segregated connections with dendritic spines of GABAergic medium spiny projection neurons (MSNs) in the striatum (Alexander et al., 1986; Alexander et al., 1990; Hoover and Strick, 1993; Parent and Hazrati, 1995). From the MSNs, striatal projections are sent to the GPi and the SN reticulata (SNr), which provide basal ganglia output to the thalamus and brainstem. These output nuclei tonically inhibit thalamocortical neurons through high rates of GABAergic discharge (DeLong, 1990; Wichmann and DeLong, 2003; Wichmann and DeLong, 2007).

Connections between the striatum and the GPi/SNr are organized into a direct and indirect pathway. The direct pathway consists of a monosynaptic connection between striatal MSNs and the GPi and SNr, whereas the indirect pathway comprises multiple synaptic connections, the first of which links striatal MSNs to the GPe. Subsequent projections in the indirect pathway link the GPe to the GPi and SNR, both directly and indirectly via the STN. Normally, striatal dopamine release increases activity of the direct pathway MSNs by stimulating dopamine D1 receptors, while decreasing activity of indirect pathway MSNs via D2 receptors. Thus, under normal conditions, the release of dopamine in the striatum results in a net reduction

of activity in the GPi and SNr through both monosynaptic or polysynaptic connections of the direct and indirect pathway neurons, respectively. Disruption of activity in these pathways impacts the functioning of the basal ganglia, including its control over motor behavior. In PD, depletion of striatal dopamine increases activity of the indirect pathway and decreases output from direct pathway MSNs. Increased inhibition of GPe neurons via indirect striatal MSNs thus disinhibits the STN, GPi, and SNr. Consequently, unusually increased inhibitory projections from the GPi and SNr to thalamic targets may abnormally increase the tonic inhibition of thalamocortical neurons and decrease motor behavior (see Fig. 1) (Albin et al., 1989; DeLong, 1990; Wichmann and DeLong, 2003; Wichmann and DeLong, 2007).

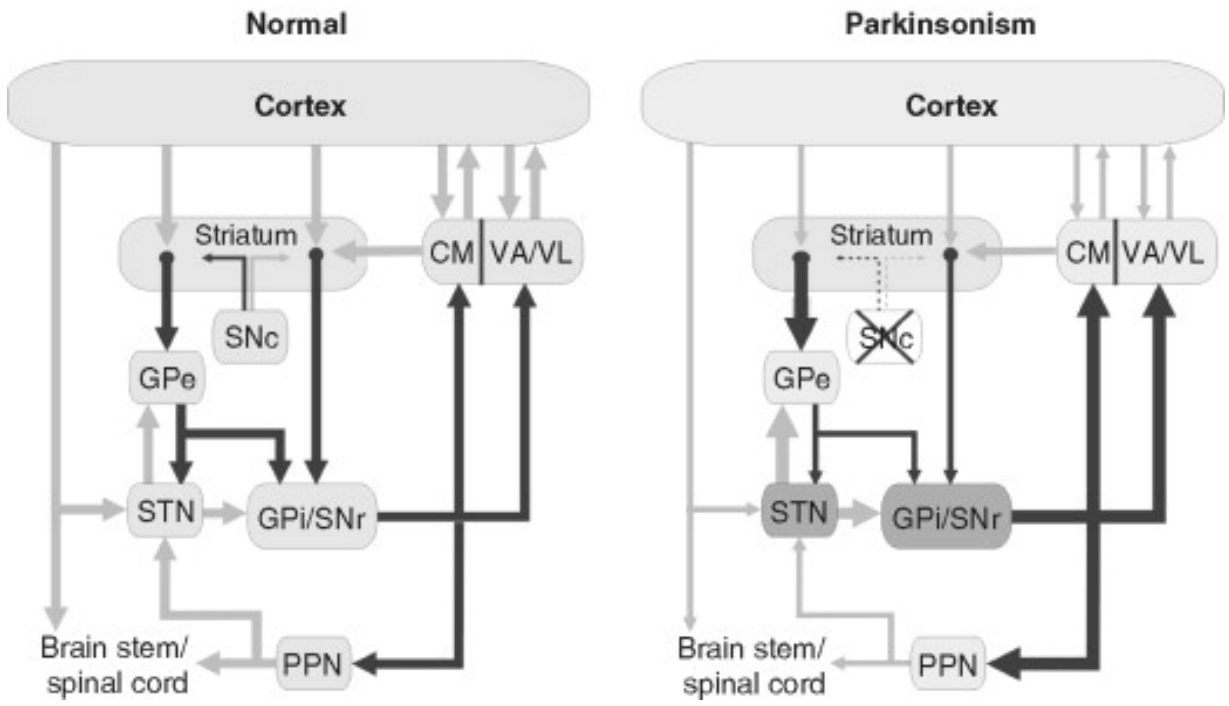

Figure 1. Activity in the basal ganglia-thalamocortical loop in the normal and parkinsonian state.

Black arrows denote inhibitory connections and gray arrows depict excitatory connections. The thickness of arrows indicates the level of activity (Wichmann and DeLong, 2007).

Organization of the Basal Ganglia-Receiving Thalamic Nuclei

The main thalamic targets of basal ganglia projections from the GPi and SNr are the ventral motor and caudal intralaminar thalamic nuclei, which are the focus of this thesis. The dorsal region of the thalamus is divided into several thalamic nuclear groups by the internal medullary lamina. Among these groups, the ventral anterior (VA) and ventral lateral (VL) comprise the motor thalamus. Specifically, the parvocellular region of the VA nucleus (VApc) receives inputs from the GPi and premotor cortex and modest innervation from the cerebellum, while the posterior ventrolateral nucleus (VLp) predominantly receives afferent connections from the deep cerebellar nuclei (Ilinsky, 1990; Ilinsky et al., 1993; Ilinsky et al., 1997; Kultas-Ilinsky et al., 1997). The VApc sends efferent connections preferentially to the premotor, supplementary motor, and prefrontal cortices, with more modest inputs to the primary motor cortex, while the opposite is true for VLp, i.e. it innervates mainly the primary motor cortex, with lighter projections to premotor and supplementary motor cortices (Jones, 2007). The intralaminar nuclei—an additional thalamic nuclear group—lie within the boundaries of the internal medullary lamina in the thalamus. These diffusely-projecting nuclei are subdivided into rostral and caudal parts. The caudal group includes the centromedian and parafascicular nuclei (CM/Pf complex) (Jones, 2007; Smith and Sidibe, 2003), which are major targets of basal ganglia outputs from the GPi and SNr. In primates, single GPi neurons send axon collaterals to both the VApc and CM, suggesting that the two thalamic targets receive common inputs from the basal ganglia (Sidibe et al., 1997; Sidibe et al., 2002; Smith et al., 2004; Parent and Hazrati, 1995).

CM/Pf neurons are the main source of thalamostriatal projections in primates. In rodents, the caudal intralaminar complex does not comprise a CM per se, but the lateral sector of the Pf nucleus corresponds to the primate CM, while the medial Pf corresponds to the primate Pf (Berendse and Groenewegen, 1990; Deschenes et al., 1996a,b; Francois et al., 1991; McFarland and Haber, 2000; McFarland and Haber, 2001; Lacey et al., 2007; Parent and Parent, 2005; Raju et al., 2006; Sadikot et al., 1992a,b; Smith and Parent, 1986; Smith et al., 2004, 2009). Tracing studies in monkeys revealed that CM/Pf neurons provide massive topographically organized projections to specific striatal areas, while giving rise to lighter inputs to the cerebral cortex (Galvan and Smith, 2011; Parent and Parent, 2005; Sadikot et al., 1992a). Overall, the CM/Pf in primates topographically projects to all functional striatal regions and thus comprises a highly

organized circuitry that might impact both motor and non-motor aspects of basal ganglia functioning (Galvan and Smith, 2011; Smith et al., 2004, 2009, 2010).

The CM receives inputs from motor, premotor, and somatosensory cortices (Catsman-Berrevoets and Kuypers, 1978; DeVito and Anderson, 1982; Kunzle, 1976, 1978; Kuypers and Lawrence, 1967). In contrast, the Pf mainly receives innervation from the frontal and supplementary eye fields (Huerta et al., 1986; Leichnetz and Goldberg, 1988) and associative parietal areas (Ipekchyan, 2011). The CM/Pf complex, moreover, receives significant input from subcortical areas, such as the superior colliculus (Grunwerg et al., 1992; Redgrave et al., 2010) and the cerebellum (Ichinohe et al., 2000; Royce et al., 1991).

As described above, the CM/Pf complex also receives prominent GABAergic innervation from collaterals of GPi and SNr neurons that project to the VApc (Sidibe et al., 1997; Sidibe et al., 2002; Smith et al., 2004; Parent and Hazrati, 1995). Pallidal axons from the sensorimotor GPi terminate entirely in the CM and form synapses with thalamostriatal neurons that project back to the sensorimotor striatum. On the other hand, associative inputs from the GPi terminate mostly in the dorsolateral Pf, while the limbic GPi innervates the rostrodorsal part of Pf, which in turn projects back to the associative and limbic striatal regions, respectively. Thus, the CM/Pf complex is part of a functionally separated basal ganglia-thalamostriatal loop in primates that integrates sensorimotor, associative, and limbic information (Sidibe et al., 2002; Smith et al., 2004; Smith et al., 2009).

CM/Pf Degeneration in PD

It is important to consider that CM, but not VApc, undergoes profound neuronal degeneration in PD (Brooks and Halliday, 2009; Halliday, 2009; Halliday et al., 2011; Henderson et al., 2000a,b, 2005). Postmortem examinations of Parkinson's disease patient brains, indeed, revealed that PD pathology involves cell death in systems other than the nigrostriatal dopaminergic projection (Braak et al., 2003; Fornai et al., 1997a,b, 2007; Gai et al., 1991; Halliday et al., 1990; Hirsch et al., 1987; Jellinger, 1988; Marien et al., 1993; Masilamoni et al., 2010, 2011; Rommelfanger et al., 2007; Rommelfanger and Weinshenker, 2007). Degeneration of non-dopaminergic cell groups is likely involved in the development of non-motor symptoms characterized by autonomic, psychiatric, and cognitive deficits in PD patients (Cools et al., 2001; Williams-Gray et al., 2006). In particular, cell loss in the thalamus (including CM/Pf) may contribute more to the pathophysiology of PD than previously thought. Postmortem

studies have demonstrated a 30-40% loss of CM/Pf neurons in PD patients with either mild or severe motor deficits, indicating that the degree of neuronal loss in these nuclei is not related to the severity of parkinsonian motor symptoms (Brooks and Halliday, 2009; Halliday, 2009; Heinsen et al., 1996; Henderson et al., 2000a,b, 2005; Smith et al., 2011, 2014; Xuereb et al., 1991).

Significant CM/Pf neuron loss has also been established in monkeys treated with chronic, low doses of the neurotoxin 1-methyl-4-phenyl-1,2,3,6-tetrahydropyridine (MPTP). In this model, neuronal degeneration is even observed in motor asymptomatic animals with partial loss of the nigrostriatal dopamine system (Villalba et al., 2014). Thus, in agreement with the postmortem human data, it appears that CM/Pf degeneration arises relatively early and is not related to the severity of motor symptoms in both PD patients and chronically MPTP-treated monkeys (Villalba et al., 2014). Based on evidence that similar degrees of cell loss have been seen across individual monkeys treated chronically with MPTP (Villalba et al., 2014), the chronically MPTP-treated monkeys may represent a valuable animal model to evaluate the functional consequences of CM/Pf degeneration in PD pathophysiology, especially in the manifestation of early non-motor deficits (Villalba et al., 2014). Interestingly, diffuse CM/Pf neuronal loss has also been observed in other neurodegenerative diseases, such as progressive supranuclear palsy and Huntington's disease (Heinsen et al., 1996; Henderson et al., 2000a,b). The mechanism underlying CM/Pf neurons' greater vulnerability to neurodegeneration than other thalamic nuclei in PD and other disorders remains unknown and warrants further study.

Changes in the Rate and Patterns of Neuronal Activity in the Basal Ganglia-Thalamocortical Loop in PD

Prior studies have described abnormal firing rates in the STN, GPi, and SNr of animal models of parkinsonism and PD patients (Brown, 2007). Recordings from thalamic cells in the VApc of MPTP-treated monkeys (Guehl et al., 2003; Kammermeier et al., 2016; Pessiglione et al., 2005) and PD patients (Magnin et al., 2000; Molnar et al., 2005; Vitek et al., 1994; Zirh et al., 1998) also revealed increased irregular firing in the thalamus. Abnormally synchronized neuronal firing is observed throughout the basal ganglia-thalamocortical circuitry in the parkinsonian state, which strikingly differs from the lack of synchronized activity and strict functional segregation within the basal ganglia nuclei and thalamus in the normal state (Hammond et al., 2007). Studies have demonstrated increased frequency and length of bursts

following dopamine depletion in PD patients and animal models (Hutchison et al., 1994; Magnin et al., 2000; Wichmann and Soares, 2006). Neural activity in the basal ganglia-thalamocortical network is therefore significantly impaired in the parkinsonian state. However, the underlying cellular and neuroplastic substrates of these changes remain largely unknown. The main goal of this thesis is to examine whether ultrastructural changes in the morphology of synapses established by GPi terminals on thalamic cells might contribute to the pathophysiology of the pallidothalamic GABAergic connection in parkinsonian monkeys.

Morphological and Structural Changes in the Pallidothalamic System in PD

A recent study from our lab demonstrated that the prevalence and overall pattern of synaptic connectivity of GABAergic terminals from the GPi in both the VApc and CM was not changed in parkinsonian monkeys (Swain et al., 2017), despite extensive CM cell death in parkinsonian animals (Villalba et al., 2014). However, because the relative GPi terminal density calculated in this study was based on terminal profile counts from single electron microscopy (EM) ultrathin sections, these findings did not take into account possible morphological changes (i.e. changes in terminal volume and shape) GPi terminals may undergo in the parkinsonian state. Because such structural changes may increase (in the case of increased terminal volume) or decrease (in the case of decreased terminal volume) the likelihood of randomly counting individual terminal profiles through single EM sections, it is important to rigorously determine if the morphology of GPi terminals is affected in parkinsonian animals. It is noteworthy that ultrastructural alterations in axon terminals have been associated with neuroplastic changes of the physiological characteristics and transmitter release properties of other terminal subtypes in various brain regions under normal and diseased conditions (Bell et al., 2014; Bourne and Harris, 2008; Bromer et al., 2018; Deutch et al., 2007; Fiala et al., 2002; Harris and Kater, 1994; Ingham et al., 1989, 1998; Kuwajima et al., 2012; Stephens et al., 2005; Suarez et al., 2016; Villalba et al., 2009, 2015; Villalba and Smith, 2010, 2011a, b, 2013; Yuste and Bonhoeffer, 2001; Zaja-Milatovic et al., 2005), including various basal ganglia nuclei in rodent and primate models of PD.

For example, previous studies have found evidence of pruning and morphological changes in corticostriatal and corticosubthalamic terminals in non-human primate and rodent models of parkinsonism (Chu et al., 2017; Day et al., 2006; Deutch, 2006; Ingham et al., 1998; Mathai et al., 2015; Raju et al., 2008; Villalba et al., 2009, 2015; Villalba and Smith, 2010,

2011). Other studies showed structural plasticity in the number of GABAergic synapses from the external globus pallidus (GPe, in primates) onto single STN neurons in rodent models of PD (Fan et al., 2012). The authors demonstrated that the increased number of synapses formed by single GPe terminals was associated with a significant increase in the strength of pallidosubthalamic GABAergic synapses in the parkinsonian state (Chu et al., 2017; Fan et al., 2012). Because GPi and GPe GABAergic terminals share common ultrastructural and functional characteristics, it is possible that similar structural alterations affect GABAergic pallidothalamic terminals in MPTP-treated parkinsonian monkeys.

Multi-synaptic Arrangement of GPi and Other GABAergic Thalamic Terminals

Data collected from GABAergic terminals that are morphologically similar to pallidothalamic terminals revealed that these multisynaptic boutons display a high level of morphological heterogeneity in terminal size and in the arrangement of synapses in the thalamus (Bodor et al., 2008; Bokor et al., 2005; Halassa and Acsady, 2016; Rovo et al., 2012; Wanaverbecq et al., 2008). In a recent 3D electron microscopic study, Bodor et al. (2008) demonstrated key ultrastructural features of nigrothalamic terminals in the ventromedial (VM) nucleus of the rat thalamus and the motor thalamus of the macaque monkey. Similar to GPi terminals, these boutons are large in size, contain a large amount of mitochondria and vesicles, and form multiple synapses with their postsynaptic targets (Bodor et al, 2008). Analysis of single electron microscopic sections in several other studies have shown that nigrothalamic terminals establish multiple synapses (Kultas-Ilinsky and Ilinsky, 1990; Kuroda and Price, 1991; Sakai et al., 1998; Tsumori et al., 2002). By forming multiple symmetric and closely-spaced synapses on a single postsynaptic target, these terminals create a favorable environment for intersynaptic spillover of GABA among the many synapses of a single bouton. This unique arrangement of active zones produces a larger charge transfer due to slower decay of synaptic currents and also decreases variability in synaptic transmission (DiGregorio et al., 2002). Such efficient GABAergic signaling endows these terminals with the ability to maintain high tonic inhibitory drive upon targets in the thalamus (Bodor et al., 2008).

Single-section electron microscopic studies of GABAergic pallidothalamic terminals show that single GPi terminals also innervate their postsynaptic target with multiple synapses (Ilinsky and Kultas-Ilinsky, 1990; Ilinsky et al., 1997; Kultas-Ilinsky and Ilinsky, 1990). This synaptic arrangement of pallidothalamic terminals ultimately may contribute to the increased

GABAergic tone imposed upon thalamocortical neurons by GPi inputs in the state of parkinsonism. Having such knowledge is essential for a deeper understanding of the functional significance of altered GPi output to thalamocortical neurons in parkinsonism.

Serial Block-Face Scanning Electron Microscopy and 3D Reconstruction to Examine Ultrastructural Changes in Pallidothalamic Terminals of Parkinsonian Monkeys

The most rigorous approach to carefully assess changes in ultrastructural features of neuronal elements, including axon terminals, is through the use of three-dimensional electron microscopy reconstruction of individual neuronal profiles. The resolution of light microscopy is not adequate to reconstruct synaptic neural circuits and precisely estimate the morphology and size of certain dendritic and axonal processes. Only EM provides a high-enough spatial resolution to clearly identify synapses and sufficiently characterize neuronal processes (Denk and Horstmann, 2004). To reliably examine ultrastructural features of axon terminals, including the size of synapses formed by GPi terminals, the current study thus necessitates the use of EM over other microscopy techniques. Furthermore, single-section EM analysis does not provide sufficient information about terminal morphology or the number, size, and arrangement of synapses, given that these structural features can span through dozens of serial sections. Because this information is essential to understand neurotransmitter dynamics and postsynaptic target responses, serial section EM reconstructions are needed to adequately measure structural parameters potentially affecting synaptic plasticity and physiology. Methods other than serial section EM would overlook ultrastructural changes possibly implicated in the altered functioning of these terminals in the parkinsonian state.

We have therefore applied serial EM reconstruction in this project to reconstruct single GABAergic terminals from the GPi in the VApc and CM of control and parkinsonian rhesus monkeys. To do so, we used the cutting-edge technology of serial block-face scanning electron microscopy (SBF/SEM). This method yields a large quantity of serial images from small regions of interest and allows for the complete 3D reconstruction of large terminals and their associated synaptic circuitry (Briggman and Denk, 2006; Fiala, 2005; Harris et al., 2006; Knott et al., 2008). 3D EM reconstruction of neural tissue has traditionally been performed with serial section transmission electron microscopy (SSTEM) of ultrathin sections. SSTEM is a simple technique but involves a tedious and error-prone sectioning process with several inherent problems, such as

loss of sections, uneven section thickness, debris on sections, and distortions that interfere with proper alignment and reconstruction of neuronal structures (Briggman and Denk, 2006).

SBF/SEM is an alternative method with many advantages over SSTEM that make reconstructing neural structures more precise and feasible. In contrast to SSTEM, images produced through SBF/SEM are generated from back-scattered electrons off the surface of a resin-embedded tissue sample. This makes imaging the block face possible and eliminates problems with section distortion or section loss during tissue handling. Also, images used in SBF/SEM datasets are already aligned and thus allow for a fully automated sectioning process that quickly and efficiently generates large volumes of images. Indeed, by incorporating a custom microtome into an SEM chamber, several hundred serial sections of thicknesses as little as 30 nm are routinely imaged in a short period of time. On the other hand, most studies using SSTEM have not been able to generate sections thinner than 50 nm, a resolution not high enough for the accurate reconstruction of very thin neuronal structures (Briggman and Denk, 2006).

3D EM reconstruction with the SBF/SEM technique therefore provides a unique opportunity to correlate underlying neural functioning with circuit-specific ultrastructural features. In this thesis, I will determine if GPi terminals in VApc and CM—the major thalamic targets in the pallidothalamic system—undergo ultrastructural changes in parkinsonian monkeys. I will also compare the synaptic microcircuitry of GPi terminals in the normal state and assess potential differences in ultrastructural changes these terminals undergo in the parkinsonian state between the two nuclei. Given that VApc and CM are innervated by the same GPi neurons, but only CM undergoes significant neuronal degeneration in MPTP-treated parkinsonian monkeys (see above), it is possible that ultrastructural features of GPi terminals in VApc and CM are affected differently in parkinsonian monkeys. Furthermore, in light of previous data from single EM sections suggesting that GPi terminals in the monkey VApc and CM display a different ultrastructure (Sadikot et al., 1992; Sidibe et al., 1997), a detailed comparative analysis of ultrastructural features of GPi terminals between the VApc and CM of control and parkinsonian monkeys using 3D EM imaging will set a solid foundation to assess structure-function relationships of these terminals in the VApc and CM in the normal and parkinsonian state.

Study Goals

This study aims to further understand the anatomical substrates through which GPi terminals may mediate effects upon thalamic cells in normal monkeys and to determine if this

connection is structurally altered in the parkinsonian state. Using high-resolution 3D EM reconstruction, changes in the volume and in the number and size of GABAergic synapses made by individual GPi terminals in the VApc and CM will be compared between control and parkinsonian monkeys. Specifically, we will measure and compare the volume of individual reconstructed GPi terminals and the number and surface area of single synapses made by these terminals in the VApc and CM of normal and parkinsonian monkeys. In light of the previous literature suggesting an increased GABAergic outflow from the GPi upon the thalamus in PD, we predict that the volume and the number and size of synapses formed by single GPi terminals will increase in the VApc and CM of MPTP-treated parkinsonian monkeys.

Materials and Methods

Animals

Two adult rhesus macaque monkeys (Macaca mulatta; MR240R and MR271L) obtained from the Yerkes National Primate Research Center were used in the study. All animal procedures have been approved by the Institutional Animal Care and Use Committee (IACUC) of Emory University, and were performed according to the Guide for the Care and Use of Laboratory Animals and the U.S. Public Health Service Policy on the Humane Care and Use of Laboratory Animals. Various members in the Smith lab performed the surgery, perfusion, behavioral assessment, and treatment of these animals before I got access to the tissue for my study.

MPTP Treatment and Assessment of Parkinsonism

One monkey used in the study was rendered parkinsonian after weekly MPTP injections (0.2-0.8 mg/kg i.m.; cumulative doses: 2.8–26.79 mg/kg; Natland International, Morrisville, NC or Sigma, St. Louis, MO) until it reached a moderate level of parkinsonism. The regimen of MPTP intoxication and the behavioral approaches used to assess the state of parkinsonian motor signs in these monkeys are described in detail in previous studies from our laboratory (Devergnas et al., 2014; Galvan et al., 2010; Masilamoni et al., 2010, 2011; Wichmann et al., 2001; Wichmann and Soares, 2006). Briefly, the severity of parkinsonian symptoms was evaluated by weekly testing of the monkey for 15-minute durations in an observation cage and measuring the number of movements with infrared break-beam sensors. A parkinsonism rating scale was also used to quantify deficits in the following motor behaviors: speed, incidence and severity of freezing episodes, extremity and trunk posture, presence and severity of tremor,

amount of arm and leg movements, finger dexterity, home cage activity, and balance. Each item was given a score from 0-3 with a maximum total score of 30. The severity of these parkinsonian motor symptoms was stable for at least 6 weeks after the last MPTP injection before the monkey was deemed parkinsonian.

Anterograde Labeling of Pallidothalamic Terminals

The control and MPTP-treated monkeys used in the study received viral vector injections (2-8 μl) of AAV5-hSyn-ChR2-EYFP or AAV5-hSyn-Arch3-EYFP in the GPi to identify pallidothalamic terminals in the VApc and CM. Labeled pallidothalamic terminals from these injections and unlabeled putative GPi terminals forming at least two symmetric axo-dendritic synapses in a single section were used for 3D EM reconstruction.

In the control monkey, the injection was introduced with a microsyringe into the ventrolateral GPi while the animal was placed in a stereotaxic frame. Pre-operative MRI scans helped delineate the stereotaxic coordinates. In the MPTP-treated monkey, recording chambers were stereotactically directed at the pallidum on both sides of the brain and attached to the skull. After surgery, electrophysiological mapping was conducted to help define the borders of the GPe and GPi using protocols formerly described from our laboratory. The injection was delivered into the GPi using a probe combined with a recording microelectrode (Kliem and Wichmann, 2004). Extracellular recordings were performed while lowering the microsyringe to determine the final location in the GPi for the injection (Galvan et al., 2010; Kliem et al., 2007).

Both monkeys survived at least 6 weeks after the virus injections to allow efficient anterograde transport to GPi terminals in the thalamus.

Tissue Collection and Processing for Microscopy

The monkeys were euthanized with pentobarbital (100 mg/kg, i.v.) and transcardially perfused with a Ringer's solution and a mixture of paraformaldehyde (4%) and glutaraldehyde (0.1%). The brains were removed, post-fixed in 4% paraformaldehyde, and cut in 50 μm serial sections with a vibratome for immunohistochemical localization of the tag protein, enhanced yellow fluorescent protein (EYFP). Sections were stored at -20°C in an anti-freeze solution until further histological processing.

Before immunohistochemistry processing, tissue samples from the VApc and CM were pre-treated with 1% sodium borohydride in a phosphate buffer for 20 minutes and subsequently washed in phosphate-buffered saline (PBS). Sections were prepared for electron microscopy and

placed in a cryoprotectant solution (phosphate buffer [PB]= 0.05 M at pH 7.4, with 25% sucrose and 10% glycerol) for 20 minutes, frozen at -80°C for 20 minutes, thawed, and returned to a graded series of cryoprotectant solution (100%, 70%, 50%, 30%) diluted in PBS. Sections were washed in PBS and then pre-incubated in a solution of 10% normal goat serum and 1% bovine serum albumin in PBS for 1 hour.

Sections were immunostained for Green Fluorescent Protein (GFP), an antibody that identifies GPi terminals anterogradely labeled in the VApc and CM with the viral vector described above. This tissue was incubated with a primary rabbit antibody (1:5,000 dilution) for 48 hours at 4°C. Next, sections were rinsed in PBS and transferred for 1.5 hours to a solution with a secondary biotinylated goat anti-rabbit antibody (1:200 dilution). After, sections were placed in a solution of 1% avidin-biotin-peroxidase complex (Vector Laboratories, Burlingame, CA USA), washed in PBS and Tris buffer (0.05 M, pH 7.6), and transferred to a solution containing 0.01M imidazole, 0.005% hydrogen peroxide, and 0.025% 3,3′-diaminobenzidine tetrahydrochloride (DAB; Sigma, St. Louis, MO) in Tris for 10 minutes. Several rinses of the tissue in PBS ended the DAB reaction.

Sections with the maximum amount of GFP immunostaining were put into vials in phosphate buffer solution and sent to Renovo Inc. (Cleveland, OH, USA) for additional EM processing (osmium fixation, dehydration, and resin embedding). After embedding, small regions of interest in the VApc and CM with dense GFP-labeled GPi terminals were removed from slides for 3D reconstruction using the SBF/SEM method. In this approach, a scanning electron microscope scans serial images from a block of tissue put on an ultramicrotome and back-scattered electrons help detect the tissue embedded in resin. The ultramicrotome cuts thin sections from the face of the block and raises the sample back to the focal plane to image the sample again. The technology samples thousands of images by scanning and cutting the tissue with this automatic process (Briggman and Bock, 2012; Denk and Horstmann, 2004)

The MPTP administration, assessment of parkinsonian motor symptoms, intracerebral injection of viral vectors, and perfusion of the animals were conducted by members of the Smith lab before I used the brain tissue from these animals for the completion of work presented in this thesis. My main contribution to this work has been the collection and analysis of 3D EM data from GFP-immunostained sections in the VApc and CM of the two animals used in this study.

3D Reconstruction from Serial Section Electron Microscopy

Select areas in the VApc and CM with dense GFP-labeled GPi terminals were used for 3D reconstruction employing the SBF/SEM method. Approximately 200-400 serially-scanned micrographic images (~70 nm-thick) were collected from each region of interest, and labeled and unlabeled GPi terminals were chosen at random from these images to be reconstructed using the 3D software *Reconstruct* (available at: synapses.clm.utexas.edu). In order to avoid bias in the selection of elements being reconstructed, I was blinded to the treatment (control vs. MPTP-treated) of each of the two animals. Identification of axon terminal subtypes in the VApc and CM was based on ultrastructural features previously reported in EM studies of the mammalian motor thalamus (Ilinsky et al., 1997; Jones, 2007; Kultas-Ilinsky et al., 1997) and in an EM study from our laboratory (Swain et al., 2017, 2018). Small (i.e. ~0.5-0.7 μm in diameter) terminals forming asymmetric synapses were categorized as originating from the cerebral cortex ("As" type); medium-to-large sized (~0.5-1.5 μm in diameter) terminals forming single symmetric synapses were considered as GABAergic terminals from the thalamic reticular nucleus (RTN; "S1" type); and large terminals enriched in mitochondria (~1-3 μm in diameter) forming multiple symmetric synapses with single postsynaptic targets were categorized as GABAergic terminals from the GPi ("S2" type). Using these structural criteria, we considered some unlabeled large multisynaptic terminals in the VApc and CM as putative GPi terminals and added those to the sample of GPi boutons reconstructed in this study (see Fig. 2 for terminal subtype classification).

TIFF images of single sections were imported into *Reconstruct* and calibrated with the section thickness and pixel size provided by Renovo. Finally, labeled and unlabeled terminals, synapses, and dendrites from each object analyzed were manually traced in each serial electron micrograph using *Reconstruct* (Villalba and Smith, 2010, 2011). From these serially identified elements, the software created a 3D representation of each object from which it calculated the volume of terminals and the surface area of synapses. The volume of terminals and the size and number of synapses were randomly recorded in control and MPTP-treated monkeys. The surface area of synapses was calculated by multiplying the trace length and section thickness. Only terminals that could be seen through their full extent in serial sections were reconstructed; a series of 30-100 scanned ultrathin images were used depending on the size of terminals. From GFP-immunostained VApc sections, 10 randomly-chosen labeled and unlabeled GPi terminals from 1 normal and 1 MPTP-treated monkey were used for 3D reconstruction. From CM sections,

13 randomly-chosen labeled and unlabeled GPi terminals from the same MPTP-treated monkey and 10 from the same control monkey were used for 3D reconstruction. To assess possible differences in the pattern of synaptic connectivity of GPi terminals in the VApc and CM between control and parkinsonian animals, the postsynaptic targets contacted by GPi terminals were categorized as large (>1.0 μm in diameter), medium (0.5-1.0 μm), or small (<0.5 μm) dendrites. Three random sections from reconstructed dendrites in synaptic contact with each of the reconstructed GPi terminals in the VApc and CM were chosen to estimate the cross-sectional diameter of postsynaptic targets and to categorize the dendrite's size according to the above criteria.

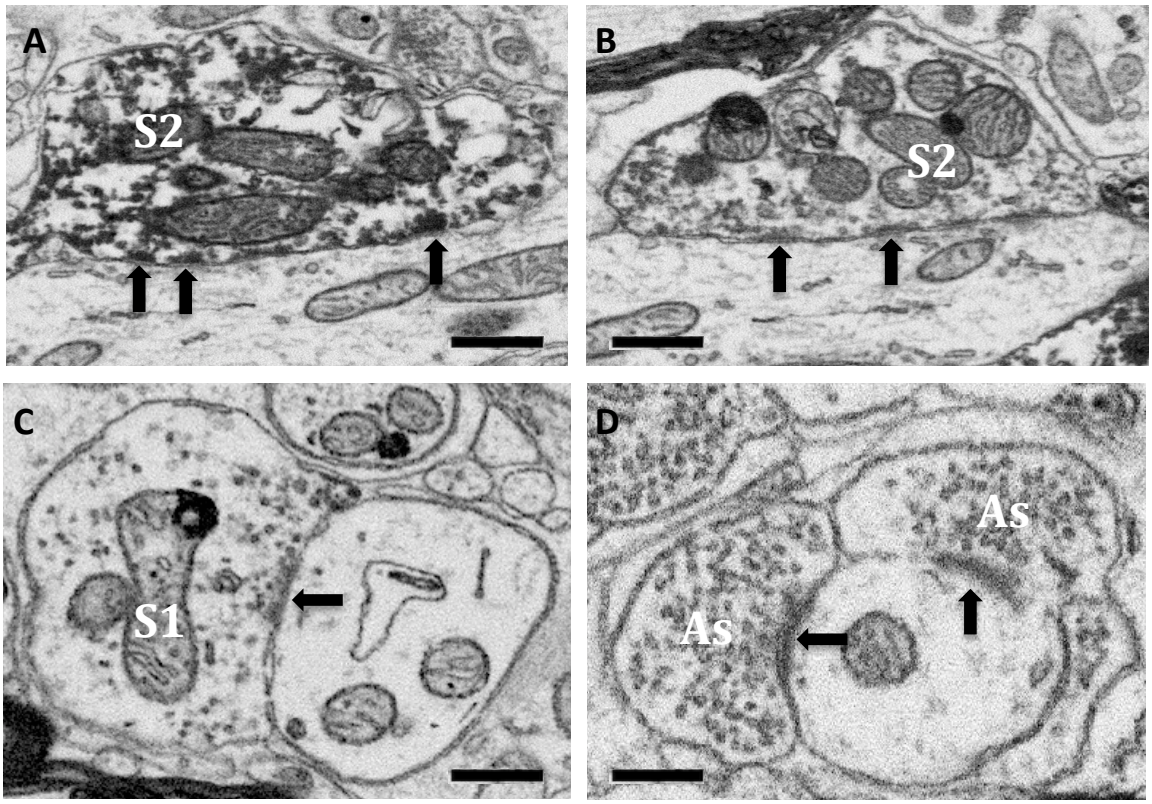

Figure 2. Classification of terminal subtypes in the VApc and CM of control and MPTP-treated monkeys.

Electron micrographs displaying the classification of terminals in the VApc and CM used to identify putative unlabeled GPi-like terminals. Top panel shows two S2 type terminals that originated from the GPi and make multiple symmetric synapses (indicated by arrowheads) on a postsynaptic target in the VApc of an MPTP-treated monkey. **(A)** shows a GFP-labeled GPi terminal. **(B)** shows an unlabeled putative GPi-like terminal**. (C)** identifies an S1 type terminal that likely originates from the RTN and makes one symmetric synapse on a single postsynaptic target in the CM of an MPTP-treated monkey. **(D)** displays an As type terminal that mainly originates from the cortex and forms a single asymmetric synapse onto a postsynaptic target in the CM of an MPTP-treated monkey. *Scale bar* =2 μm

Statistical Analysis

Statistical analysis was performed using SigmaStat (version 2.03; Aspire Software International, Ashburn, VA). For terminal volume, number of synapses per terminal, and surface area of synapses, data were compared by a student's t-test or Mann-Whitney test (depending on results of the normality test) to determine statistical differences between control and MPTP-treated monkeys and between the VApc and CM in both the control and MPTP conditions. For all statistical tests, "n" was chosen as the number of GPi terminals.

Results

Ultrastructural Features of Pallidothalamic Terminals in the VApc of a Control and MPTP-treated Parkinsonian Monkey

The ultrastructural features of GPi terminals were assessed to determine if terminal volume, synapse surface area, and the number of synapses differed between normal and MPTP-treated monkeys and between the VApc and CM in both conditions. In the VApc, a total of 20 GFP-labeled and unlabeled GPi terminals and their respective postsynaptic targets and synapses were 3D-reconstructed in a control (n=10; 4 GFP-labeled, 6 unlabeled) (Fig. 3a-c) and an MPTP-treated monkey (n=10; 8 GFP-labeled, 2 unlabeled) (Fig. 4a-c). Occasionally, more than one GPi terminal formed synapses with a single dendrite (Fig. 4a). The terminal volume, surface area of synapses, and the average number of synapses per GPi terminal were measured and averaged from each monkey.

In the control monkey, the median volume of GPi terminals was 10.39 μm^3 (mean: 10.79 μm^3; n=10), whereas the median terminal volume was 14.17 μm^3 in the MPTP-treated monkey (mean: 13.82 μm^3; n =10). Although there was a trend toward increased GPi terminal volume in the MPTP-treated animal, the difference was not statistically significant (Fig. 5a; p=0.252, student's t test). The surface area of the synapses formed by GPi terminals was significantly increased in the MPTP-treated monkey (Fig. 5b; p=0.021, Mann-Whitney test). In the control monkey, the median surface area was 0.10 μm^2 (mean: 0.096 μm^2; n=10), whereas the median was 0.14 μm^2 in the MPTP-treated monkey (mean: 0.15 μm^2; n =10). The average number of synapses per GPi terminal was significantly lower in the MPTP-treated monkey than in the control animal (Fig. 5c; control: mean, 16.6; median, 14.0; n =10; MPTP: mean, 10.1; median, 11; n =10; p=0.050, student's t-test). In the majority of cases, single GPi terminals made multiple

synaptic connections with the same postsynaptic target. One of the 10 reconstructed terminals in the control monkey and 3 of 10 terminals in the MPTP-treated monkey formed multiple synapses onto two or more different postsynaptic targets. The cross-sectional diameters of dendritic profiles contacted by GPi terminals in the VApc of control and MPTP-treated monkeys were tabulated. Consistent with data from a previous study from our laboratory (Swain et al., 2017, 2018), they were of the medium and large-sized category (Table 1).

This preliminary quantitative analysis of 3D-reconstructed pallidothalamic terminals in the VApc suggests that the volume of GPi terminals and the area of synapses formed by these terminals may be larger, while the average number of synapses formed by individual terminals may be smaller in the MPTP-treated monkey than in the control (Fig. 5a-c). Future studies that include more animals in both groups and additional terminals from the same monkeys should be achieved to confirm these preliminary observations.

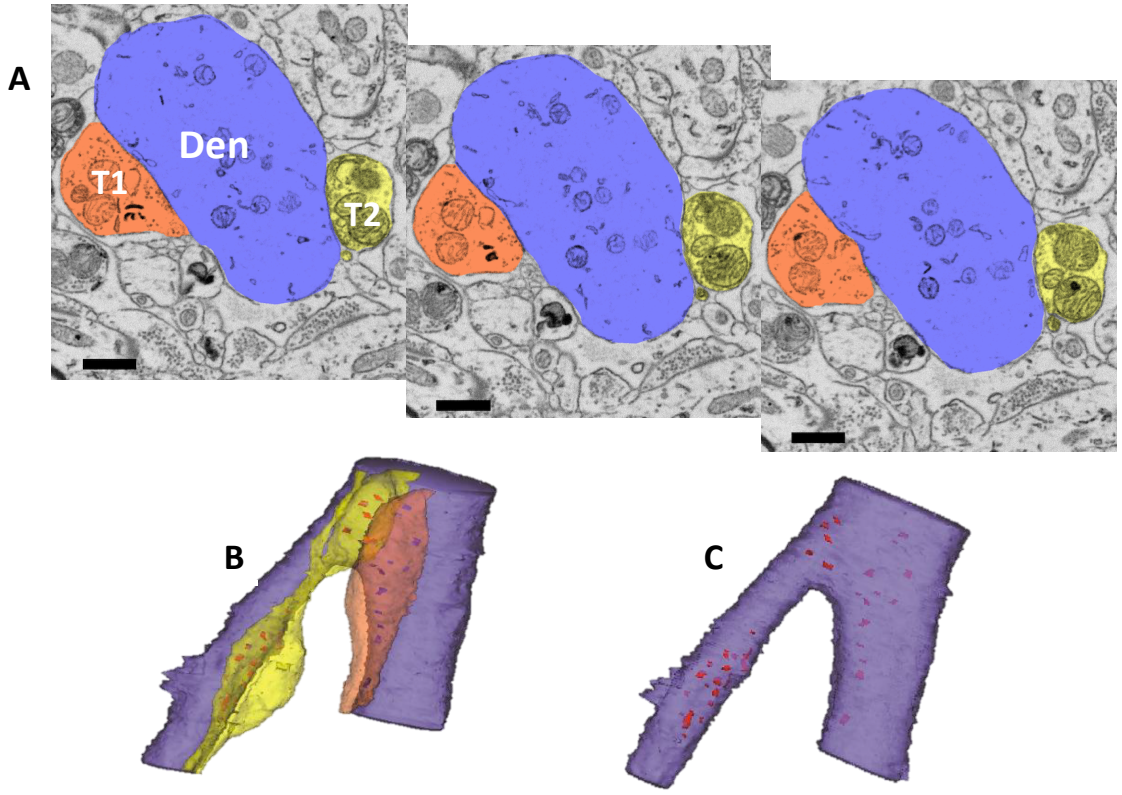

Figure 3. Pallidothalamic terminals forming multiple synapses with a large dendrite in the VApc of a control animal.

(A) Serial electron micrographs of two GPi terminals (T1-orange, T2-yellow) in contact with a large dendrite (Den-purple) in the VApc of the control monkey. T2 displays GFP immunoreactivity indicating that it was anterogradely labeled by the AAV injection in the GPi. **(B)** 3D reconstructed images of T1, T2, the postsynaptic dendrite, and the symmetric synapses (red shapes) formed by the two terminals. In **(C)**, only the symmetric axo-dendritic synapses (red shapes) formed by T1 and T2 are shown. *Scale bar* =2 µm in **(A)**.

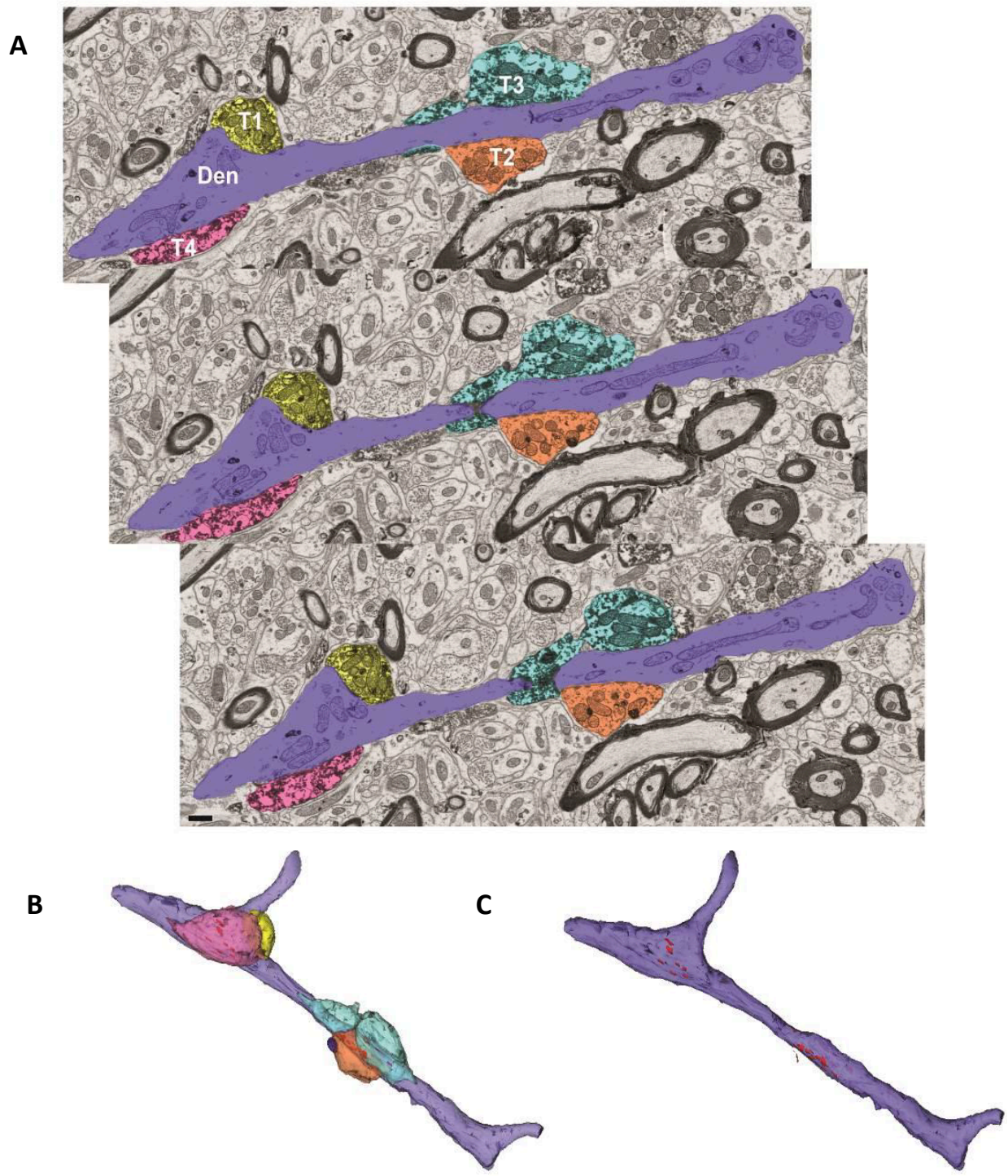

Figure 4. Pallidothalamic terminals in contact with a large dendrite in the VApc of an MPTP-treated monkey.

(A) Serial electron micrographs of four GFP-immunostained GPi terminals (T1-yellow, T2-orange, T3-blue, and T4-pink) in contact with a single large dendrite (Den-purple) in the VApc. **(B-C)** 3D reconstruction of the four terminals and their postsynaptic dendrite. The multiple symmetric synapses formed by single terminals can be seen in partially transparent images of the terminals in **(B)**. In **(C)**, terminals have been removed from the image to better illustrate the morphology and density of the symmetric synapses formed by T1, T2, T3, and T4. *Scale bar* =2μm in **(A)**.

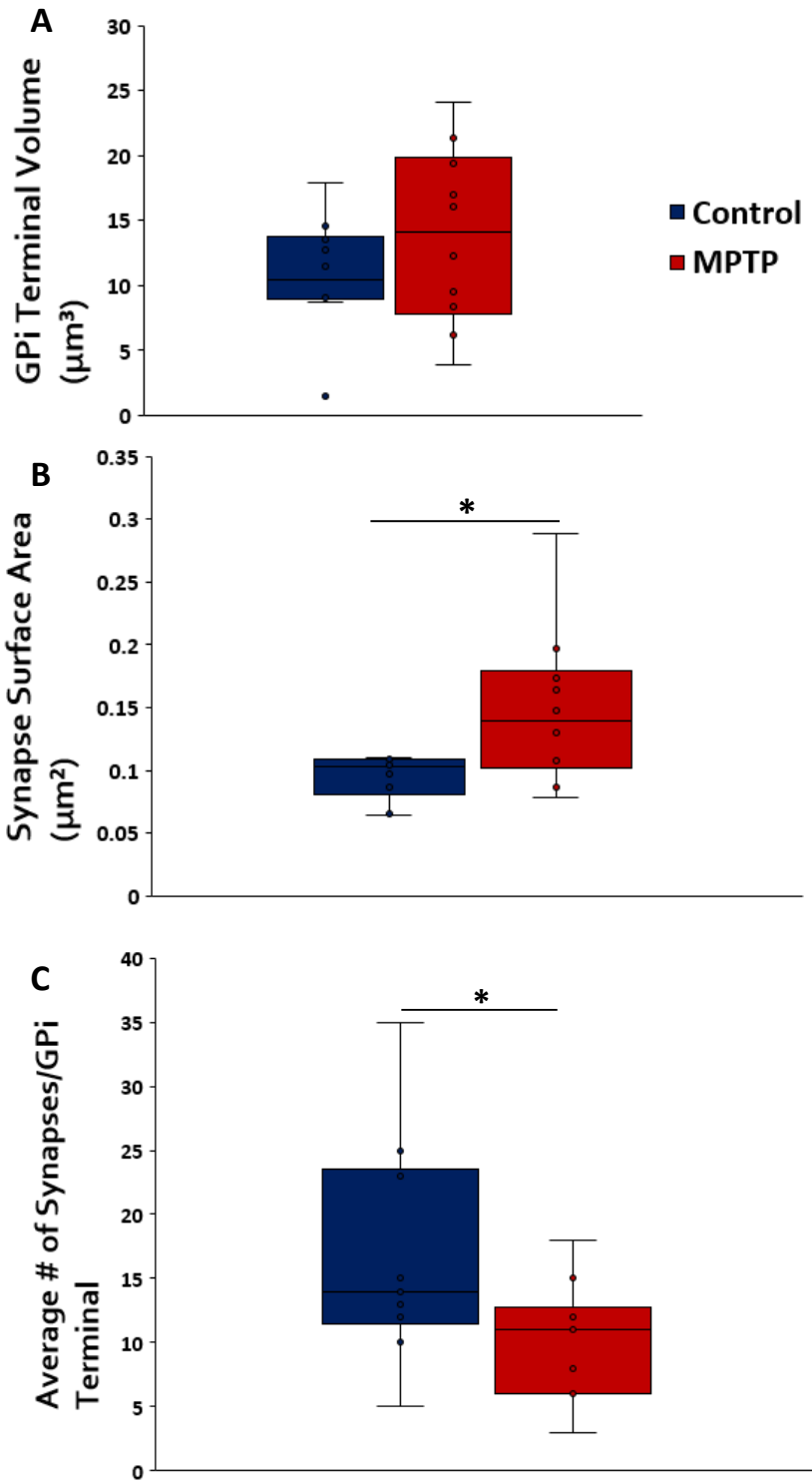

Figure 5. Quantification of ultrastructural features of pallidothalamic terminals in the VApc of control and MPTP-treated monkeys.

(A-C) Box-whisker plots comparing the morphometric measurements (GPi terminal volume, synapse surface area, and average number of synapses per GPi terminal) of structural elements at pallidothalamic GABAergic synapses using 3D reconstruction of single GPi terminals from serial ultrathin images. A total of 10 terminals in each group from one control and one MPTP-treated animal were used. The units used for these measurements are indicated in the Y-axis within parenthesis. **(A)** The mean GPi terminal volume is not significantly different between the MPTP monkey and the control. **(B)** In an MPTP monkey, the mean synapse surface area is significantly larger than the control (***,** $P \leq 0.05$, Mann-Whitney test, n= number of GPi terminals). **(C)** In a control monkey, the mean number of synapses per GPi terminal is significantly larger than the MPTP monkey (*, $P \leq 0.05$, student's t-test, n= number of GPi terminals).

Ultrastructural Features of Pallidothalamic Terminals in the CM of a Control and MPTP-treated Parkinsonian Monkey

In the CM, a total of 23 GFP-labeled and unlabeled GPi terminals and their respective postsynaptic targets and synapses were 3D-reconstructed in a control (n=10; 2 GFP-labeled, 8 unlabeled) (Fig. 6a'-b') and MPTP-treated monkey (n=13; 6 GFP-labeled, 7 unlabeled) (Fig. 6c'-d'). The terminal volume, surface area of synapses, and the average number of synapses per GPi terminal were measured and averaged from each monkey.

The GPi terminal volume was significantly increased in the parkinsonian monkey (Fig. 7a; p=0.014, Mann-Whitney test). In the control monkey, the median volume of GPi terminals was 2.61 μm^3 (mean: 2.96 μm^3; n =10), while in the MPTP-treated monkey, the median terminal volume was 4.38 μm^3 (mean: 5.85 μm^3; n =13). The surface area of the synapses of GPi terminals was also significantly increased in the MPTP-treated monkey (Fig. 7b; p=0.010, Mann-Whitney test). In the control monkey, the median surface area was 0.13 μm^2 (mean: 0.14 μm^2, n =10), whereas the median was 0.21 μm^2 in the MPTP-treated monkey (mean: 0.21 μm^2; n =13). Also, the average number of synapses per GPi terminal was significantly higher in the MPTP-treated monkey than in the control (Fig. 7c; control: mean, 5.5; median, 6; n =10; MPTP: mean, 9.62; median, 9; n =13; p=0.013, Mann-Whitney test). In the majority of cases (11/13 terminals), GPi terminals made multiple synaptic connections on the same postsynaptic target in the MPTP-treated monkey. Two terminals simultaneously formed multiple synapses onto two or more different postsynaptic targets. On the other hand, 6/10 terminals in the control monkey simultaneously converged on more than one postsynaptic target. The cross-sectional diameters of dendritic profiles contacted by GPi terminals in the CM of control and MPTP-treated monkeys were tabulated. Consistent with data presented from a previous study from our laboratory (Swain et al., 2017, 2018), they were of the medium and large-sized category (Table 1).

This preliminary quantitative analysis of 3D-reconstructed pallidothalamic terminals in the CM suggests that the volume of GPi terminals as well as the number and area of synapses formed by these terminals may be larger in MPTP-treated monkeys than in controls (Fig. 7a-c). Studies with additional animals and terminals in each group must be completed to confirm these preliminary observations.

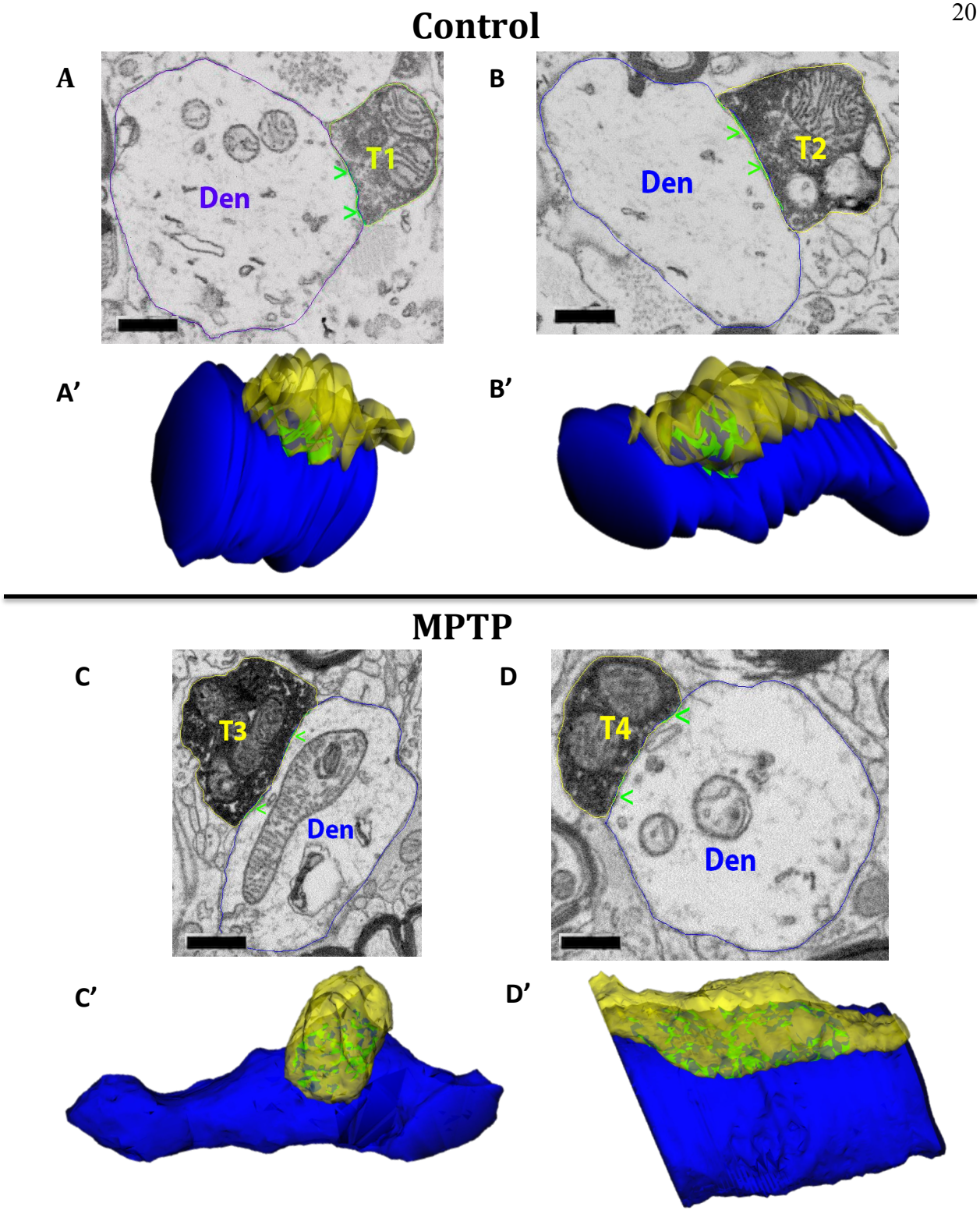

Figure 6. Pallidothalamic terminals forming synapses with a dendrite in the CM of a control and MPTP-treated monkey.

(A-B; C-D) Electron micrographs of anterogradely labeled GPi terminals (T-yellow) in contact with a dendrite (Den-blue) in the CM of a control (T1 and T2 at top) and MPTP-treated (T3 and T4 at bottom) monkey. Each terminal displays GFP immunoreactivity indicating anterograde labeling by the AAV injection in the GPi. Green arrowheads point at symmetric axo-dendritic synapses. **(A'-B'; C'-D')** 3D reconstruction of the four anterogradely labeled terminals (yellow), their postsynaptic dendritic targets (blue), and the axo-dendritic symmetric synapses (green) in a partially transparent image of the GPi terminals to allow visualization of the symmetric synapses. *Scale bar* =2 μm

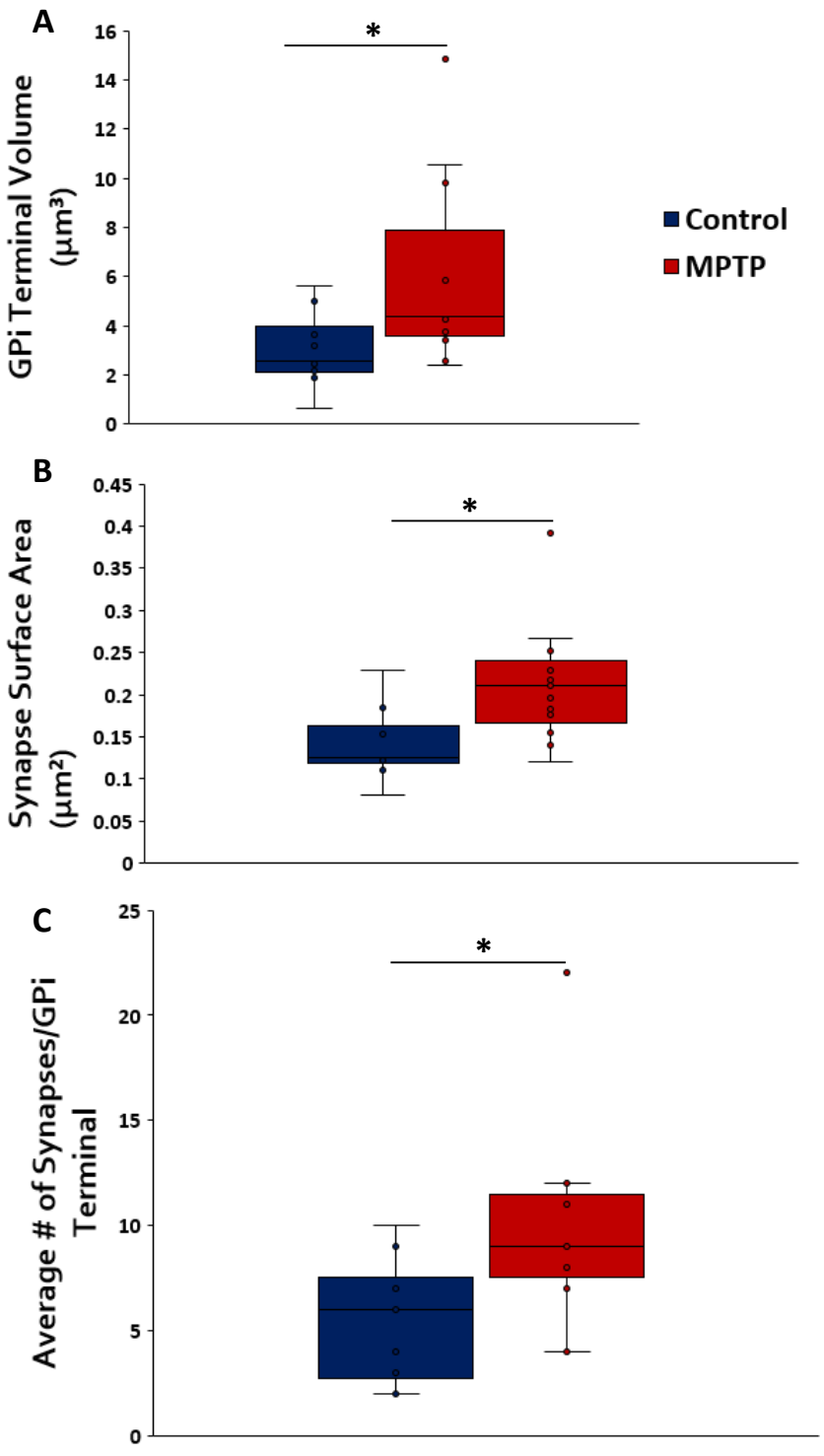

Figure 7. Quantification of ultrastructural features of pallidothalamic terminals in the CM of control and MPTP-treated monkeys.

(A-C) Box-whisker plots comparing the morphometric measurements (GPi terminal volume, synapse surface area, and average number of synapses per GPi terminal) of structural elements at pallidothalamic GABAergic synapses using 3D reconstruction of single GPi terminals from serial ultrathin images. A total of 10 terminals from one control and 13 terminals from one MPTP-treated animal were used. The units used for these measurements are indicated in the Y-axis within parenthesis. **(A)** In an MPTP monkey, the mean GPi terminal volume is significantly larger than the control (*****, $P \leq 0.05$, Mann-Whitney test, n= number of GPi terminals). **(B)** In an MPTP monkey, the mean synapse surface area is significantly larger than the control (*****, $P \leq 0.05$, Mann-Whitney test, n= number of GPi terminals). **(C)** In an MPTP monkey, the mean number of synapses per GPi terminal is significantly larger than the control (*****, $P \leq 0.05$, Mann-Whitney test, n= number of GPi terminals).

Table 1. Postsynaptic target distribution of GPi terminals in the VApc (top) and CM (bottom) of a control and MPTP-treated monkey.

VApc		Average Dendrite Diameter (µm)	Dendrite Category
Control	T1	1.00	Medium
	T2	1.99	Large
	T3	1.22	Large
	T4	0.68	Medium
	T5	1.36	Large
	T6	2.10	Large
	T7	2.70	Large
	T8	2.98	Large
	T9	0.96	Medium
	T10	1.71	Large
MPTP	T1,T3,T4	1.69	Large
	T2	1.53	Large
	T5	1.04	Large
	T6	1.30	Large
	T7	0.93	Medium
	T8	1.22	Large
	T9	1.73	Large
	T10	0.83	Medium

CM		Average Dendrite Diameter (µm)	Dendrite Category
Control	T1	2.62	Large
	T2	0.87	Medium
	T3	0.76	Medium
	T4	0.68	Medium
	T5	0.53	Medium
	T6	0.58	Medium
	T7	0.75	Medium
	T8	0.73	Medium
	T9	1.25	Large
	T10	0.58	Medium
MPTP	T1	2.31	Large
	T2	2.95	Large
	T3	1.87	Large
	T4	2.25	Large
	T5	2.74	Large
	T6	1.54	Large
	T7	0.97	Medium
	T8	1.66	Large
	T9	1.16	Large
	T10	0.83	Medium
	T11	0.62	Medium
	T12	0.76	Medium
	T13	1.84	Large

Comparison of Ultrastructural Features of Pallidothalamic Terminals between the VApc and CM of a Control and MPTP-treated Monkey

From a total of 20 GPF-labeled and unlabeled GPi terminals and their respective postsynaptic targets and synapses that were 3D-reconstructed in a control monkey from both the VApc (n=10 terminals) and the CM (n=10 terminals), the average terminal volume, surface area of synapses, and the number of synapses per GPi terminal were compared between nuclei. The volume of GPi terminals was significantly larger (Fig. 8a) in the VApc (median: 10.39 μm^3; mean: 10.79 μm^3; n =10) than in the CM (median: 2.61 μm^3; mean: 2.96 μm^3; n =10); (p=0.002, Mann-Whitney test). The surface area of synapses formed by GPi terminals was significantly larger (Fig. 8b) in the CM (median: 0.13 μm^2; mean: 0.14 μm^2; n=10) than in the VApc (median: 0.10 μm^2; mean: 0.096 μm^2; n=10) (p=0.006, student's t-test). However, the average number of synapses per GPi terminal was significantly higher (Fig. 8c) in the VApc (mean: 16.6; median: 14; n=10) compared to the CM (mean: 5.5; median: 6; n =10) (p=0.001, student's t-test).

From a total of 23 GPF-labeled and unlabeled GPi terminals and their respective postsynaptic targets and synapses that were 3D-reconstructed in an MPTP-treated monkey from both the VApc (n=10 terminals) and the CM (n=13 terminals), a similar inter-nuclear comparison was completed for the MPTP-treated monkey. The volume of GPi terminals was significantly larger (Fig. 9a) in the VApc (median: 14.17 μm^3; mean: 13.82 μm^3; n=10) than in the CM (median: 4.38 μm^3; mean: 5.85 μm^3; n=13) (p=0.002, student's t-test). The surface area of synapses formed by GPi terminals was significantly larger (Fig. 9b) in the CM (median: 0.21 μm^2; mean: 0.21 μm^2; n=13) than in the VApc (median: 0.14 μm^2; mean: 0.15 μm^2; n =10) (p=0.024, Mann-Whitney test). No significant differences were found for the average number of synapses per GPi terminal (Fig. 9c) between the VApc and CM (p=0.801, student's t-test).

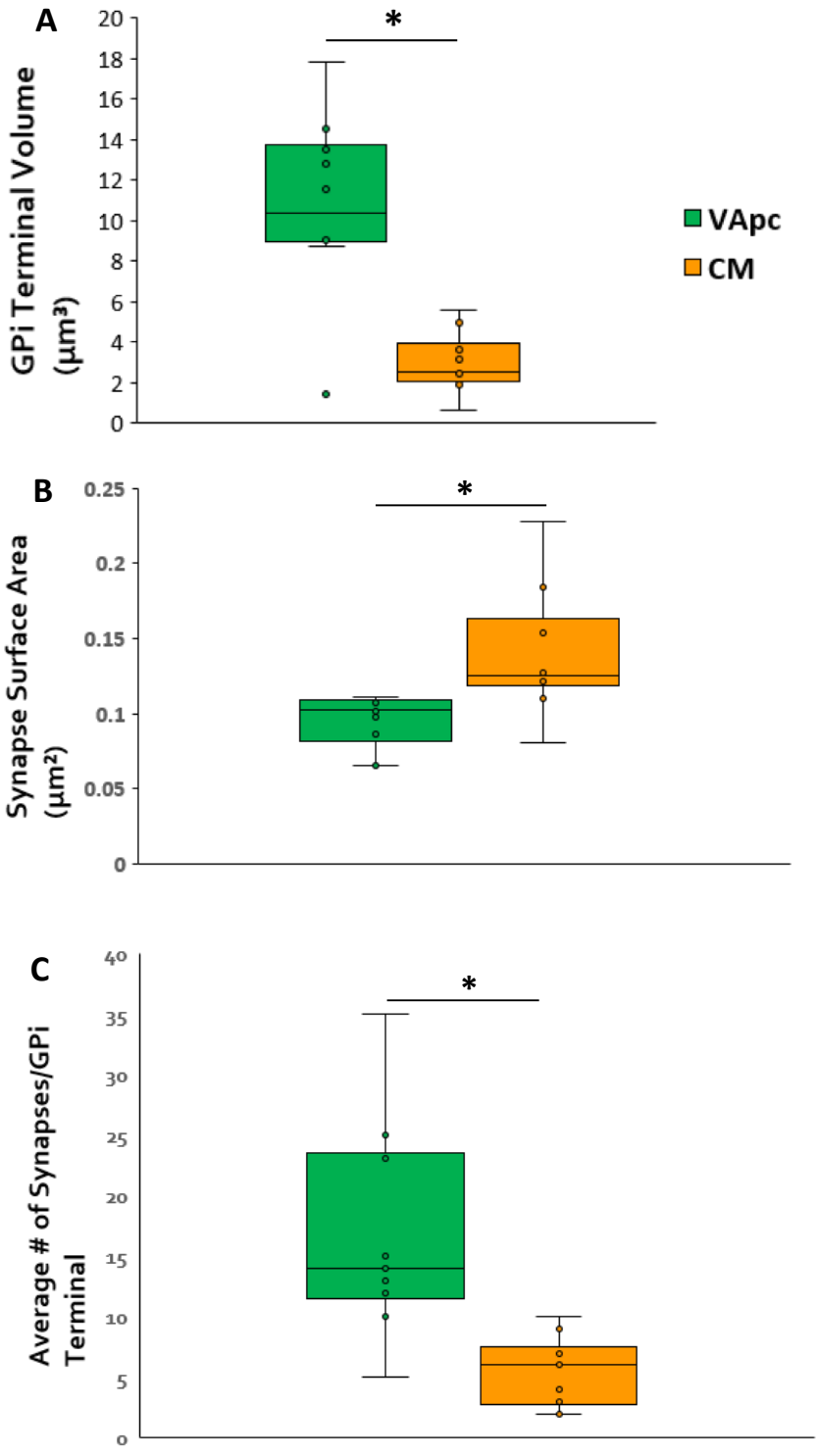

Figure 8. Comparison of ultrastructural features of pallidothalamic terminals between the VApc and CM of control monkeys.

(A-C) Box-whisker plots comparing the morphometric measurements (GPi terminal volume, synapse surface area, and average number of synapses per GPi terminal) of structural elements at pallidothalamic GABAergic synapses between the VApc and CM using 3D reconstruction of single GPi terminals from serial ultrathin images. The units used for these measurements are indicated in the Y-axis within parenthesis. **(A)** The mean GPi terminal volume is significantly larger in the VApc than in the CM (*****, $P \leq 0.05$, Mann-Whitney test, n= number of GPi terminals). **(B)** The mean synapse surface area is significantly larger in the CM than in the VApc (*****, $P \leq 0.05$, student's t-test or Mann-Whitney test, n= number of GPi terminals). **(C)** The mean number of synapses is significantly larger in the VApc than in the CM (*****, $P \leq 0.05$, student's t-test, n= number of GPi terminals).

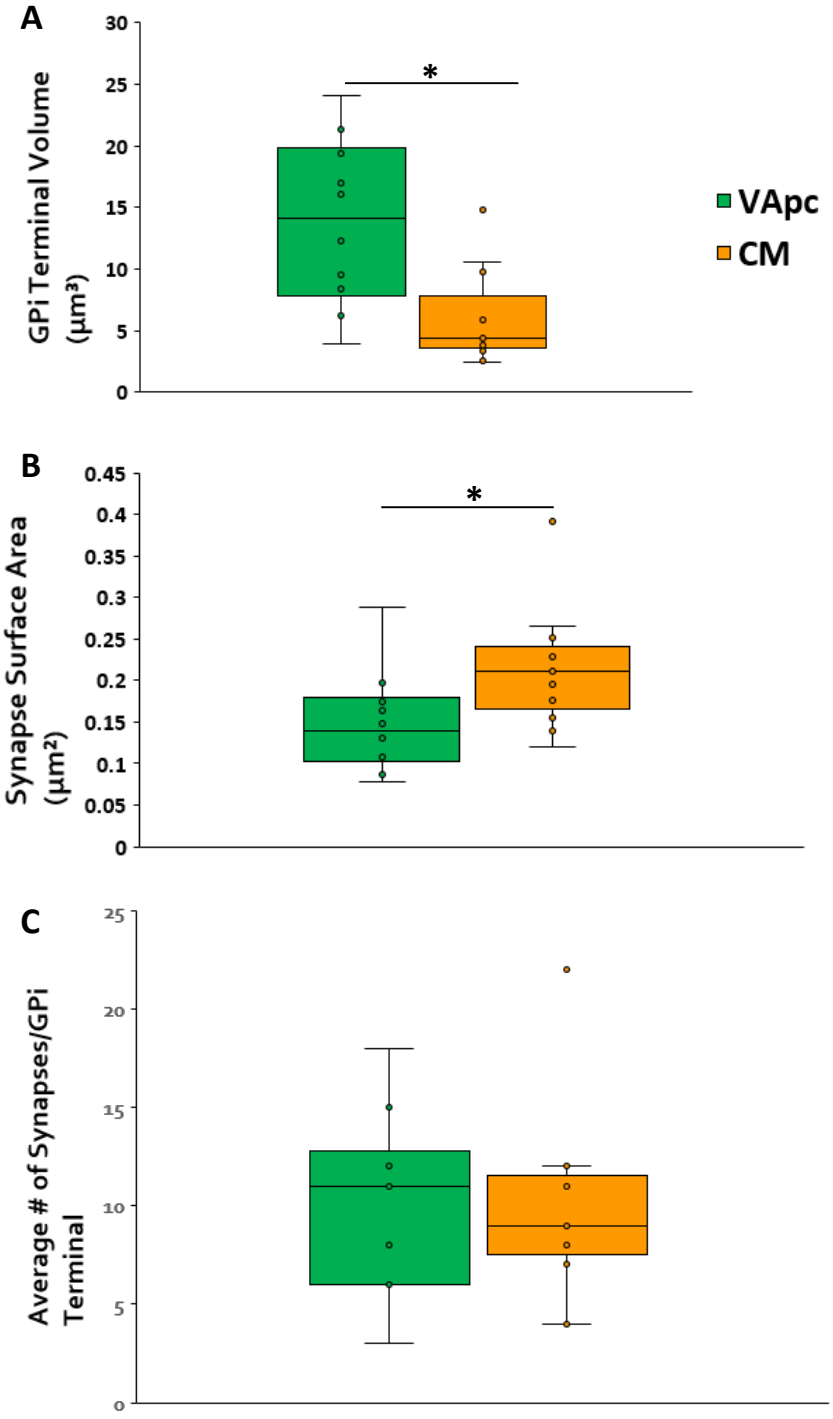

Figure 9. Comparison of ultrastructural features of pallidothalamic terminals between the VApc and CM of MPTP-treated monkeys.

(A-C) Box-whisker plots comparing the morphometric measurements (GPi terminal volume, synapse surface area, and average number of synapses per GPi terminal) of structural elements at pallidothalamic GABAergic synapses between the VApc and CM using 3D reconstruction of single GPi terminals from serial ultrathin images. The units used for these measurements are indicated in the Y-axis within parenthesis. **(A)** The mean GPi terminal volume is significantly larger in the VApc than in the CM (***,** $P \leq 0.05$, student's t-test, n= number of GPi terminals). **(B)** The mean synapse surface area is significantly larger in the CM than in the VApc (***,** $P \leq 0.05$, student's t-test or Mann-Whitney test, n= number of GPi terminals). **(C)** The mean number of synapses per terminal is not significantly different between the VApc and CM.

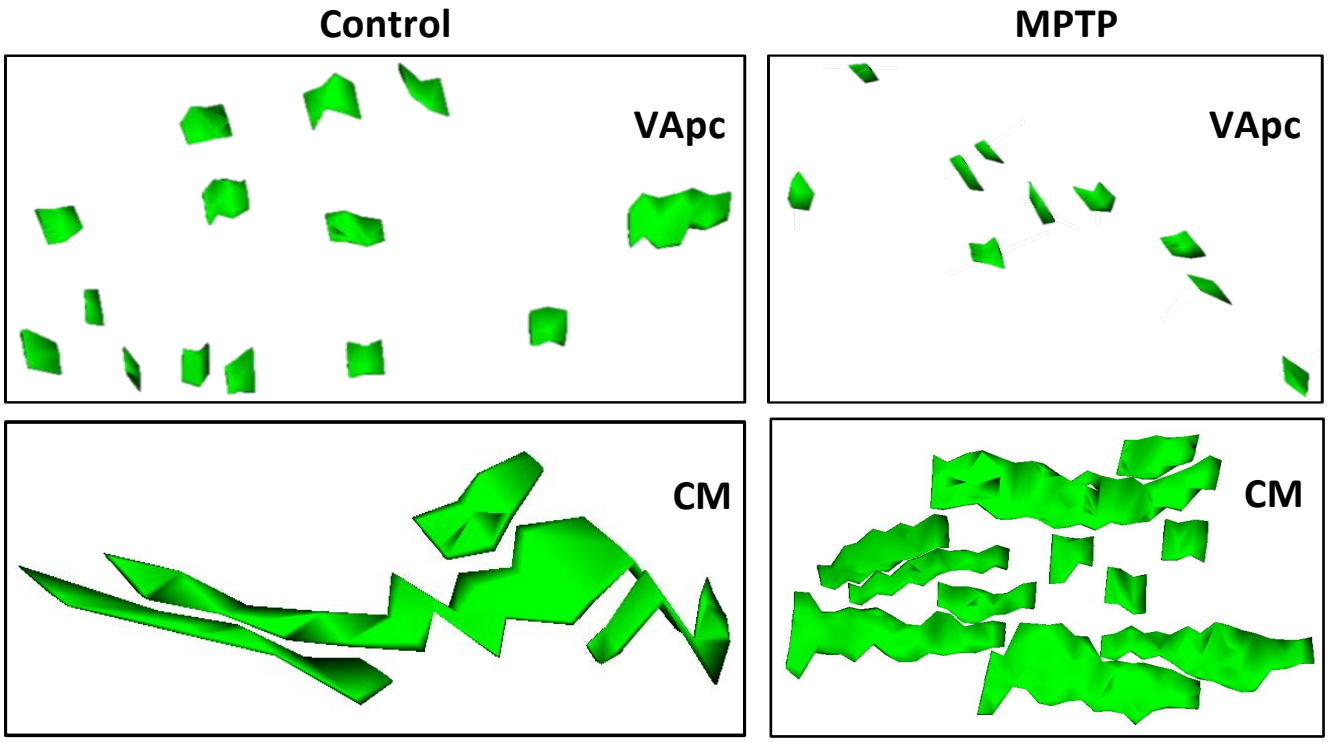

Figure 10. Comparison of 3D-Reconstructed Synapses in the VApc and CM of control and MPTP-treated monkeys.

For the control monkey (left column), 3D reconstructions show the morphology of 15 synapses in the VApc (mean #/terminal=16.6; mean surface area=0.096 μm²) and 6 synapses in the CM (mean #/terminal=5.5; mean surface area=0.14 μm²). For the MPTP-treated monkey (right column), 3D reconstructions show the morphology of 11 synapses in the VApc (mean #/terminal=10.1; mean surface area=0.15 μm²) and 9 synapses in the CM (mean #/terminal=9.6; mean surface area=0.21 μm²). Note the major structural differences between synapses formed by GPi terminals in the VApc vs. CM.

Discussion

The preliminary data presented in this thesis suggest that ultrastructural changes of GPi GABAergic terminals take place in both the VApc and CM of MPTP-treated monkeys, which may underlie functional differences in the pallidothalamic system between normal and parkinsonian conditions. Another important observation made from our study is that the structural features of GPi terminals in the VApc are strikingly different from those in the CM in both the control and parkinsonian monkey, despite the common origin of these terminals from the same GPi neurons (Sidibe et al., 1997; Sidibe et al., 2002; Smith et al., 2004; Parent and Hazrati, 1995). The observed structural changes suggest that pallidothalamic terminals are endowed with a high level of structural plasticity that may contribute to their increased tonic regulation of thalamocortical outflow in PD. Furthermore, the target-specific differences in the

ultrastructure of GPi terminals that innervate VApc vs. CM neurons may underlie physiological differences in the effects of pallidal output to these two thalamic targets in the control and parkinsonian state.

3D Reconstruction Utilizing SBF/SEM

To our knowledge, data from this and a recent study from our laboratory (Swain et al., 2018) present the first 3D reconstruction of pallidothalamic terminals in the VApc and CM of control and parkinsonian monkeys. Because of the large size of GPi terminals and the complex arrangement of active zones, single section transmission electron microscopy analysis cannot fully characterize the morphology of these elements. The need for 3D EM reconstruction of single terminals through serial sections is essential to rigorously assess and quantify the morphometry of these terminal boutons. 3D EM reconstruction through serial sections is routinely achieved through regular ultrathin sectioning and serial section transmission electron microscopy; however, technical limitations inherent to the sectioning process involved in these methods (section loss, uneven section thickness, and distortions) hamper the use of such an approach. SBF/SEM is a more precise and efficient method that quickly collects large amounts of already-aligned ultrathin (30-70nm) sections. This cutting-edge methodology allows for the complete reconstruction of complex synaptic circuits and their connectivity in the primate brain. Combined with immunolabeling techniques, 3D serial EM reconstruction offers the unique opportunity to determine circuit-specific changes in the structure of axon terminals and their associated synaptic circuitry and provides insight into the 3D morphology and distribution of synapses, which would otherwise remain undetected with other microscopy methods. Fully reconstructing synaptic networks with this approach thus rigorously addresses ultrastructural changes of GPi terminals in the VApc and CM and may help elucidate the functional significance of synaptic microcircuitry plasticity in the development and progression of Parkinson's disease pathophysiology.

Preliminary findings suggest that GABAergic pallidothalamic terminals undergo morphological changes in volume and in the number and size of synapses in the parkinsonian state. 3D serial electron microscopic reconstruction showed that single GPi terminals innervate their postsynaptic target with multiple synapses, consistent with previous observations of single and 3D electron microscopic studies of GPi or SNr GABAergic pallido- or nigro-thalamic terminals (Bodor et al., 2008; Bokor et al., 2005; Ilinsky and Kultas-Ilinsky, 1990; Ilinsky et al.,

1997; Kultas-Ilinsky and Ilinsky, 1990). Because terminal volume and the number and size of the multiple synapses formed by GPi terminals can modulate synaptic neurotransmitter release, synaptic strength, and/or neurotransmitter uptake (Bodor et al., 2008), data from this work may help understand the role of GABAergic inputs from the GPi to the thalamus and how this circuitry is altered in PD.

Specifically, one can speculate that GPi terminals of a larger volume may provide the space necessary to produce a greater number of synapses and/or form synapses of a greater area, which could result in greater total GABA release. These changes can potentially facilitate prolonged high-frequency transmission and increase pallidothalamic synaptic efficacy by enabling simultaneous activation of postsynaptic receptors. GPi terminals might also increase in volume to accommodate growing metabolic demands associated with enhanced synaptic transmission resulting from individual terminals forming synapses of a greater size or greater number. 3D reconstruction and quantitative analysis comparing the size and density of mitochondria in GPi terminals of normal vs. parkinsonian monkeys should be performed to explore this hypothesis. Moreover, individual synapses of GPi terminals might increase in surface area in parkinsonian monkeys to accommodate a greater density of GABA-A receptors and therefore create a stronger synapse.

Functional Consequences of Anatomical and Morphological Features of Axon Terminals in GABAergic and Glutamatergic Systems

Combined anatomical and physiological data have revealed the presence of large, multisite GABAergic terminals in the thalamus that exert a strong inhibitory influence on their targets (Barthó et al., 2002; Bokor et al., 2005; Halassa and Acsady, 2016; Lavallée et al., 2005; Rovo et al., 2012). Postsynaptic responses depend on the type of presynaptic terminal and the number, size, and arrangement of synapses (Cathala et al., 2005). For example, large terminals and multiple active zones are associated with large amplitude synaptic currents and faithful synaptic transmission in several brain areas (Bokor et al., 2005), including in various GABAergic thalamic afferents. For example, tract-tracing studies have identified large multisite GABAergic terminals in the rat thalamus arising from the zona incerta (Bartho et al., 2007) and anterior pretectal nucleus (APT) (Bokor et al., 2005) which were found to exert powerful control on the activity of thalamic postsynaptic targets.

The ultrastructural features of APT terminals—including their large size and multiple release sites—enable these terminals to maintain synaptic transmission at high presynaptic firing rates and to have a strong influence on neuronal activity in the thalamus (Xu-Friedman and Regehr, 2004). Indeed, a 3D EM reconstruction study of GABAergic inputs in the posterior thalamic nucleus of the rat suggests that the interaction between multiple synapses of individual APT GABAergic terminals contributes to this powerful impact on thalamocortical activity (Wanaverbecq et al., 2008). In contrast to the monosynaptic reticular thalamic nucleus (nRT) terminals, which failed to maintain tonic inhibition, activation of the multi-synaptic APT terminals generated a larger charge transfer and greater persistent current, even at high stimulation frequencies, in thalamocortical cells (Wanaverbecq et al., 2008). Results from quantal analysis indicated that cross talk among the many closely-spaced synapses of APT terminals tailors these boutons to maintain strong inhibition, whereas nRT terminals, which form single synapses onto their postsynaptic targets in the thalamus, did not show a corresponding prolonged GABA release (Wanaverbecq et al., 2008). These data offer possible explanations for the efficacy of extrareticular inhibition in controlling relay cell activity in the sensory and motor thalamus (Wanaverbecq et al., 2008). Knowledge gained from these systems can help understand the potential significance of structural changes in the morphology and synaptic incidence of GPi terminals in the VApc and CM of parkinsonian monkeys.

It is known that nigrothalamic terminals, which have a very similar morphology to APT and GPi terminals, also display a multi-synaptic morphology with closely-spaced synapses (Bodor et al., 2008). Synapses formed by GPi terminals in the CM and VApc examined in this study also tended to be closely spaced and thus, like nigrothalamic and APT terminals, may produce a favorable environment for transmitter spillover (Bodor et al., 2008). Transmitter spillover among multiple synapses of a single terminal generates a larger charge transfer resulting from slower decay of synaptic currents and reduced variability inherent in the probabilistic nature of synaptic transmission (DiGregorio et al., 2002). At the cerebellar mossy fiber-granule cell connection, for example, single AMPA receptor EPSCs are mediated by direct glutamate release and rapid spillover of glutamate from neighboring synapses. Spillover-mediated components of the EPSC show little variability in amplitude, which likely strengthens the reliability of synaptic transmission and firing rate for a given input frequency (DiGregorio et al., 2002).

Additional evidence from glutamatergic systems reveals that the specific arrangement of synapses formed by individual terminals has a strong influence on the degree of spillover and synaptic cross-talk. For instance, during development of the cerebellar cortex, synapses of the mossy fiber-granule cell connection become more separated (Cathala et al., 2005), which increases intersynaptic distance, and, combined with a decreased chance that neighboring postsynaptic densities are on the same granule cell, thereby reduces the potential impact of transmitter spillover on components of the EPSCs (Cathala et al., 2005). On the other hand, data from cerebellar Purkinje neurons in mice demonstrates that intersynaptic cross-talk between synapses of single axon terminals—mediated through GABA spillover—can maintain faithful synaptic transmission even at high-frequency firing rates (Telgkamp et al., 2004) that would normally be associated with synaptic depression when vesicle fusion exceeds the rate of vesicle replenishment (Zucker and Regehr, 2002). A 3D EM reconstruction of these Purkinje terminals showed large boutons with multiple active zones and large amounts of synaptic vesicles, suggesting that structural features of Purkinje boutons are adapted for efficient spillover-mediated transmission. This spillover-enhanced synaptic transmission maintains high frequency inhibition by allowing postsynaptic receptors to rapidly bind GABA (Telgkamp et al., 2004).

Changes in the Number and Size of GABAergic Pallidothalamic Synapses in Parkinsonian Monkeys: Potential Functional Significance

GABA release from multi-site GPi boutons in the VApc and CM may similarly limit depletion-based depression, allowing for the maintenance of prolonged, high-frequency inhibition at pallidothalamic synapses. Forming multiple synapses of a greater size may allow for even greater inter-synaptic spillover of GABA and result in prolonged inhibition of thalamocortical outflow in the parkinsonian state. Studies in rodent models of PD have indicated that GABAergic synapses from the GPe on STN neurons (Chu et al., 2017; Fan et al., 2012) undergo structural plasticity in the number of synapses that is associated with changes in the strength of pallidosubthalamic synapses. Because GPe and GPi GABAergic terminals share common features, including a large size, large number of mitochondria, and the formation of multiple synapses with postsynaptic targets (Ilinsky et al., 1997; Kultas-Ilinsky and Ilinsky, 1990; Kultas-Ilinsky et al., 1997), structural changes in the number of pallidothalamic synapses may also be associated with changes in the strength of the pallidothalamic connection in parkinsonism.

Multiple synapses on single GPi terminals may allow for cross-talk amongst synapses, which can limit vesicle depletion in a similar way as described for GABAergic synapses in the cerebellum during prolonged high-frequency simulation (Telgkamp et al., 2004). Multisite terminals may mediate this effect; the cerebellar Purkinje cells mentioned above exhibited a mean number of synapses (9.2) that is similar to previous studies in rat and monkey SNR terminals (8.5) (Bodor et al., 2008). In the present study, the multisite pallidothalamic terminals in the monkey form a comparable number of synapses—10.1 in in the VApc and 9.6 in the CM of the MPTP-treated monkey.

These structural changes are consistent with data from previous studies examining changes in the firing rate of GPi and thalamic neurons, thalamic metabolic activity, and thalamic GABA release in the parkinsonian state. In agreement with predictions from functional models of the basal ganglia circuitry in control and parkinsonian states (Fig. 1), the firing rate of GPi neurons is increased in parkinsonian monkeys (Soares et al., 2004; Wichmann et al., 1999) and PD patients (Hutchison et al., 1994). Effects of abnormally increased basal ganglia GABAergic output on thalamic firing rates have been assessed in a few studies. In normal monkeys, the firing rate of many neurons in basal ganglia-receiving areas of the thalamus was reduced after electrical stimulation of the GPi (Anderson et al., 2003). Similarly, high-frequency stimulation of the GPi in MPTP-treated monkeys resulted in lower firing rates in the ventral motor thalamus (Kammermeier et al., 2016).

Additional studies have examined neuronal activity in the ventral motor thalamus of PD patients and parkinsonian monkeys. Studies in MPTP-treated monkeys have found increased burst firing in the motor thalamus (Guehl et al., 2003; Pessiglione et al., 2005), and similarly high levels of bursting have been shown in corresponding thalamic areas in PD patients (Magnin et al., 2000; Molnar et al., 2005; Zirh et al., 1998). In addition, neurons in basal ganglia-receiving areas of the thalamus have shown a decreased firing rate in PD patients compared to recordings from healthy controls (Molnar et al., 2005). Furthermore, studies of MPTP-treated monkeys suggest an increased metabolic activity in the ventral motor thalamus (Mitchell et al., 1989; Rolland et al., 2007), possibly reflecting increased basal ganglia input. It is also known that mRNA expression of the α1 subunit of GABA-A receptors is decreased in basal ganglia-receiving areas of the thalamus in rodent models of PD (Caruncho et al., 1997; Chadha et al.,

2000), which may result from unusually increased synaptic release of GABA in the parkinsonian condition.

Our ultrastructural data offer insight into potential anatomical changes underlying the altered activity of pallidal and thalamic cells observed in the above studies. One can speculate that individual GPi terminals of a larger volume that form synapses of a greater surface area and/or a greater number of closely-spaced synapses possess structural features particularly amenable to efficient, prolonged GABAergic signaling. For example, larger GPi terminals with more and larger synapses could allow abnormally-increased firing of GPi neurons to mediate and maintain stronger tonic inhibition of thalamic cells. Specifically, greater transmitter spillover and cross-talk among the many closely-spaced synapses of these larger terminals might produce abnormally increased inhibitory output to the thalamus that underlies the observed reduction in thalamic firing rates and increased metabolic activity in the motor thalamus of MPTP-treated monkeys. Decreased GABA-A receptor mRNA expression may also arise from prolonged GPi GABA release, possibly facilitated by a greater number of GABAergic pallidothalamic synapses and/or synapses of a greater surface area that can accommodate additional GABA-A receptors. However, the functional consequences of this mRNA down regulation on the expression of GABA-A receptors in thalamic areas remains to be established.

Differences in Ultrastructural Features of Pallidothalamic Terminals in the VApc and CM of Normal and Parkinsonian Monkeys: Potential Functional Implications

Serial electron microscopy analysis confirmed observations from previous single section studies suggesting that GPi terminals in the VApc and CM have characteristically different ultrastructural features in normal monkeys (Sadikot et al., 1992; Sidibe et al., 1997). Given these differences, it is possible that the synaptic properties and physiological effects of GPi terminal activation on VApc or CM neurons differ in both control and parkinsonian states. Most interestingly, because pallidal axonal projections to the VApc and CM originate from the same GPi neurons (Sidibe et al., 1997; Sidibe et al., 2002; Smith et al., 2004; Parent and Hazrati, 1995), our findings suggest target-specific ultrastructural differences in GPi terminals.

GPi terminals in normal monkeys are, indeed, larger in volume and form more synapses onto single targets in the VApc than in the CM. The volume of GPi terminals in the VApc of MPTP-treated monkeys is increased and remains larger than that of CM terminals in the parkinsonian state, possibly suggesting that the prolonged inhibition of thalamocortical outflow

by the GPi can be more powerful and of longer duration in the VApc than in the CM of parkinsonian monkeys. However, preliminary results also suggest that the number and surface area of synapses per terminal are decreased in the VApc, but increased in the CM of parkinsonian monkeys. One may speculate that the formation of fewer closely-spaced synapses may act as a compensatory mechanism to reduce the prolonged inhibition of thalamocortical cells in the parkinsonian state. In the CM, on the other hand, forming a larger number of synapses of a greater size may allow for greater inter-synaptic spillover of GABA that exacerbates GABAergic inhibition of thalamic activity in the basal-ganglia-thalamocortical loop in this nucleus. Given that the VApc and CM are innervated by the same GPi neurons, but that the VApc does not undergo significant neuronal degeneration in MPTP-treated parkinsonian monkeys, it is possible that ultrastructural features of GPi terminals are affected differently in the VApc and CM of parkinsonian monkeys in response to this CM cell loss. Furthermore, because GPi terminals in the VApc and CM display different ultrastructural characteristics, these findings raise the possibility of a target-specific regulation of terminal morphology during brain development.

The possibility of functional differences in the VApc and CM remains to be directly tested via electrophysiological studies that activate the GPi and compare the resulting effect of these stimulations on thalamic cells in the VApc and CM. While a previous study has done so in the ventral motor thalamus of MPTP-treated monkeys (Kammermeier et al., 2016), none to our knowledge have assessed the effect of GPi stimulation on the activity of CM neurons or have compared the impact of electrical stimulation of the GPi on the activity of CM vs. VApc neurons. Such studies will provide important information about possible behavioral consequences of anatomical changes of pallidothalamic terminals and their associated synaptic microcircuitry in the thalamus and how these changes may underlie different compensatory or pathophysiological changes of the pallidothalamic GABAergic inputs to VApc vs. CM in parkinsonism.

Potential Consequences of Neuronal Degeneration on the Synaptic Innervation of CM

Although CM undergoes significant neuronal degeneration in parkinsonian monkeys (Villalba et al., 2014), a recent study from our lab found no change in the number and pattern of synaptic innervation of GPi terminals in the CM of MPTP-treated monkeys, based on single section EM counts of terminal profiles (Swain et al., 2017). In light of findings of the present

study showing that the volume of GPi terminals in CM is significantly increased in the parkinsonian monkey, we suggest that this increase in size may account for the lack of a significant difference in the density of GPi terminals assessed from single EM section observations in our recent study (Swain et al., 2017). A greater GPi terminal volume may have, indeed, increased chances of randomly counting single terminal profiles through single EM sections. It is noteworthy that increased terminal volume has also been observed in other areas undergoing significant degeneration in the parkinsonian state. For example, striatal MSNs of MPTP-treated monkeys undergo extensive spine loss. However, the remaining spines and pre-synaptic glutamatergic terminals display complex ultrastructural changes—including a larger spine volume, larger postsynaptic density, larger spine apparatus, and a larger pre-synaptic terminal. These structural changes are thought to underlie the increased synaptic activity of corticostriatal synapses in the parkinsonian state (Villalba and Smith, 2011). It is thus possible that GPi terminals innervating CM neurons spared from degeneration in parkinsonian monkeys become larger in volume to compensate for neuronal degeneration by enhancing the strength of pallidothalamic GABAergic inhibition.

As another compensatory mechanism, remaining CM neurons in MPTP-treated monkeys may also receive additional inputs from terminals that originally innervated the CM neurons that underwent degeneration. To examine this, the synaptic connectivity of individual dendrites and cell bodies of CM neurons of normal and parkinsonian monkeys must be 3D reconstructed to measure and compare the density of different types of terminals (As, S1, and S2) in contact with CM neuron dendritic and somatic profiles. This data will help determine if CM neurons spared from degeneration in the parkinsonian state undergo a reorganization of their pattern of synaptic innervation. Finding a greater density of inhibitory RTN and GPi terminals and/or a reduced density of excitatory cortical terminals forming synaptic contacts with remaining CM neurons may allude to increased thalamic inhibition and thus reduced excitatory thalamic output in dopamine-depleted animals.

Future Directions

To complete this study, additional pallidothalamic terminals (that allow for around 25 terminals per group) will be analyzed from the same control and parkinsonian monkeys. A comparable number of terminals per group from 1-2 more control and MPTP-treated monkeys that have received injections of viral vectors in the GPi will also be analyzed. The addition of

this material will increase the statistical power and allow us to confirm (or not) the preliminary findings presented in this thesis.

Because postsynaptic responses evoked in specific neurons rely on the number and size of synapses that the activated afferents provide to their target neurons (Cathala et al., 2005), it is possible that the pathophysiology of GPi inputs to the VApc and CM in parkinsonism is due to altered expression of synaptic GABA-A receptor and reuptake sites in parkinsonian animals. To directly address this issue, future studies should assess changes in the expression of GABA receptor subunits at individual pallidothalamic synapses and relate those changes to the functional properties of these synapses under normal and parkinsonian conditions.

To further address the functional significance of the structural changes described in this study on thalamic cell activity, single cell patch clamp recordings of VApc and CM neurons should be done to explore the underlying mechanisms through which these changes affect the intrinsic physiological properties and responses of these neurons to extrinsic afferents. For example, through the use of optogenetic activation of GPi terminals in the VApc and CM, in vitro patch clamp recording studies could assess changes in the number of release sites, probability of release, and quantal content of pallidothalamic synapses in the two thalamic nuclei between control and parkinsonian animals, as previously reported for thalamic GABAergic inputs from the RTN or APT in rodents (Wanaverbecq et al., 2008). However, because of the limited tools available to study synaptic physiology in primates and the large number of animals needed to achieve such studies, the feasibility of these experiments in primates is limited. Some of those could be performed in rodent models of PD, with the caveat that the organization of the pallidothalamic system differs between rodents and primates and that CM/Pf neurons do not degenerate in rodents (Smith et al., 2004, 2009).

Only a few in vivo electrophysiological studies have addressed the impact of GPi stimulation on the ventral motor thalamus in normal (Anderson et al., 2003) and MPTP-treated monkeys (Kammermeier et al., 2016), and none, to our knowledge, have examined this in CM. Electrophysiological data of CM activity in primate models of PD remains sparse, while a few investigators have conducted such studies in the Pf of dopamine-depleted rats. One study found a transient decrease in spontaneous firing rates of Pf neurons in 6-OHDA treated rats (Ni et al., 2000). It is important to consider that possible changes in CM/Pf neuronal activity in PD may arise from both altered inputs from the GPi and the fact that CM/Pf neurons degenerate early in

parkinsonism, in both PD patients (Brooks and Halliday, 2009; Halliday, 2009; Heinsen et al., 1996; Henderson et al., 2000a,b, 2005) and in MPTP-treated monkeys (Villalba et al., 2014). Because such degeneration is not seen in the 6-OHDA-treated rodent model of PD, the translation of data from this animal model to the state of human PD must be done with caution (Villalba and Smith, 2018).

Furthermore, it will be important to experimentally test if the ultrastructural changes reported in this thesis are causal or compensatory to the pathophysiology of the pallidothalamic system in the parkinsonian state. One way to address this issue would be to examine the temporal development of these ultrastructural changes and determine if they are correlated with the development of parkinsonian motor signs. To do so, two groups of MPTP-treated monkeys should be used. A first group of "*motor asymptomatic*" MPTP-treated monkeys should include monkeys with partial (~30-40%) striatal dopamine depletion that do not display parkinsonian motor symptoms. A second group of "*motor symptomatic*" monkeys should be MPTP-treated monkeys that display 60-70% striatal dopamine depletion and exhibit parkinsonian motor symptoms (as was the case for the parkinsonian monkey used in the present study). Morphological and ultrastructural changes in terminal volume and the number and size of synapses could be compared between these two groups and with control untreated animals. If structural changes similar to the ones observed in the present study arise in the symptomatic group, but not in asymptomatic animals, it would suggest that these plastic changes are likely to be associated with the development of parkinsonism and PD pathophysiology. On the other hand, if animals in the asymptomatic group display structural changes similar to those described in the present study for symptomatic animals, it will indicate that these changes are not directly linked to parkinsonian motor symptoms, but may rather be seen as changes that appear during the course of the disease to compensate for other pathophysiological insults the basal ganglia-thalamocortical circuitry undergoes.

Yet, data from such experiments remains correlational. A more causal relationship could stem from experiments testing whether dopaminergic therapies reverse some aspects of these structural changes. Pharmacological therapies will likely not reverse them, however, as structural changes most likely develop slowly and are long-lasting. Moreover, the fact that dopaminergic therapies effectively treat PD symptoms implies that the therapeutic effect of these drugs may override the potential pathological impact of structural changes. It is possible that once

dopaminergic treatments are stopped, structural changes contribute to pathology again and create a more permanent disease state by rewiring the pallidothalamic system at the synaptic level. An additional experiment could involve increasing the severity of parkinsonian symptoms by administering a higher dose or prolonging MPTP treatment and examining if structural changes become more pronounced. If these changes appear more striking with increasing disease severity, structural changes are likely causal to pathophysiology and arise with the development of motor symptoms. Ideally, if there were methods to reverse these structural changes without altering other systems, this could allow for the examination of a causal link between these plastic events and the occurrence of motor symptoms.

Overall, neuroanatomical data from the rigorous serial section EM analysis done in the present study provides critical information about the number, size, and spatial arrangement of synapses and the morphological heterogeneity of axon terminals in the primate thalamus. Having this quantitative analysis lays the foundation for future electrophysiological studies that will examine transmitter dynamics and postsynaptic responses to eventually elucidate the functional consequences of ultrastructural changes in terminal volume and the number and size of synapses of pallidothalamic terminals in Parkinson's disease pathophysiology.

References

Albin RL, Young AB, Penney JB (1989) The functional anatomy of basal ganglia disorders. Trends Neurosci 12:366-375.

Alexander GE, DeLong MR, Strick PL (1986) Parallel organization of functionally segregated circuits linking basal ganglia and cortex. Annu Rev Neurosci 9:357-381.

Alexander GE, Crutcher MD, DeLong MR (1990) Basal ganglia-thalamocortical circuits: parallel substrates for motor, oculomotor, "prefrontal" and "limbic" functions. Prog Brain Res 85:119-46.

Anderson ME, Postupna N, Ruffo M (2003) Effects of high-frequency stimulation in the internal globus pallidus on the activity of thalamic neurons in the awake monkey. J Neurophysiol 89:1150-1160.

Bartho P, Slezia A, Varga V, Bokor H, Pinault D, Buzsaki G, Acsady L (2007) Cortical control of zona incerta. J Neurosci 27:1670-1681.

Bell ME, Bourne JN, Chirillo MA, Mendenhall JM, Kuwajima M, Harris KM (2014) Dynamics of nascent and active zone ultrastructure as synapses enlarge during long-term potentiation in mature hippocampus. J Comp Neurol 522:3861-84.

Berendse HW, Groenewegen HJ (1990) Organization of the thalamostriatal projections in the rat, with special emphasis on the ventral striatum. J Comp Neurol 299:187-228.

Bodor AL, Giber K, Rovó Z, Ulbert I, Acsády L (2008) Structural correlates of efficient GABAergic transmission in the basal ganglia-thalamus pathway. J Neurosci 28:3090-102.

Bokor H, Fre`re SG, Eyre MD, Sle´zia A, Ulbert I, Lu¨thi A, Acsa´dy L (2005) Selective GABAergic control of higher-order thalamic relays. Neuron 45:929-940.

Bourne JN, Harris KM (2008) Balancing structure and function at hippocampal dendritic spines. Annu Rev Neurosci 31:47-67.

Braak H, Del Tredici K, Rub U, de Vos RA, Jansen Steur EN, Braak E (2003) Staging of brain pathology related to sporadic Parkinson's disease. Neurobiol 24:197-211.

Briggman KL, Denk W (2006) Towards neural circuit reconstruction with volume electron microscopy techniques. Curr Opin Neurobiol 16:562-570.

Briggman KL, Bock DD (2012) Volume electron microscopy for neuronal circuit reconstruction. Curr Opin Neurobiol 22:154-161.

Bromer C, Bartol TM, Bowden JB, et al. (2018) Long-term potentiation expands information content of hippocampal dentate gyrus synapses. Proc Natl Acad Sci USA 115:E2410-E2418.

Brooks D, Halliday GM (2009) Intralaminar nuclei of the thalamus in Lewy body diseases. Brain Res 78:97-104.

Brown P (2007) Abnormal oscillatory synchronisation in the motor system leads to impaired movement. Curr Opin Neurobiol 17:656-64.

Caruncho HJ, Liste I, Rozas G, Lopez-Martin E, Guerra MJ, Labandeira-Garcia JL (1997) Time course of striatal, pallidal and thalamic alpha 1, alpha 2 and beta 2/3 GABAA receptor subunit changes induced by unilateral 6-OHDA lesion of the nigrostriatal pathway. Brain Res Mol Brain Res 48:243-250.

Cathala, L Holderith NB, Nusser Z, DiGregorio DA, Cull-Candy SG (2005) Changes in synaptic structure underlie the developmental speeding of AMPA receptor-mediated EPSCs. Nat Neurosci 8:1310-8.

Catsman-Berrevoets CE, Kuypers HG (1978) Differential laminar distribution of corticothalamic neurons projecting to the VL and the center median. An HRP study in the cynomolgus monkey. Brain Res 154:359-365.

Chadha A, Dawson LG, Jenner PG, Duty S (2000) Effect of unilateral 6-hydroxydopamine lesions of the nigrostriatal pathway on GABA(A) receptor subunit gene expression in the rodent basal ganglia and thalamus. Neuroscience 95:119-126.

Chu HY, McIver EL, Kovaleski RF, Atherton JF, Bevan MD (2017) Loss of Hyperdirect Pathway Cortico-Subthalamic Inputs Following Degeneration of Midbrain Dopamine Neurons. Neuron 95:1306-1318 e1305.

Cools R, Barker RA, Sahakian BJ, Robbins TW (2001) Enhanced or impaired cognitive function in Parkinson's disease as a function of dopaminergic medication and task demands. Cereb Cortex 11:1136-1143.

Day M, Wang Z, Ding J, An X, Ingham CA, Shering AF, Wokosin D, Ilijic E, Sun Z, Sampson AR, Mugnaini E, Deutch AY, Sesack SR, Arbuthnott GW, Surmeier DJ (2006) Selective elimination of glutamatergic synapses on striatopallidal neurons in parkinson disease models. Nat Neurosci 9:251-259.

DeLong MR (1990) Primate models of movement disorders of basal ganglia origin. Trends Neurosci 13:281-285.

Denk W, Horstmann H (2004) Serial block-face scanning electron microscopy to reconstruct three-dimensional tissue nanostructure. PLoS Biol 2:e329.

Deschenes M, Bourassa J, Doan VD, Parent A (1996a) A single-cell study of the axonal projections arising from the posterior intralaminar thalamic nuclei in the rat. Eur J Neurosci 8:329-343.

Deschenes M, Bourassa J, Parent A (1996b) Striatal and cortical projections of single neurons from the central lateral thalamic nucleus in the rat. Neuroscience 72:679-687.

Deutch AY (2006) Striatal plasticity in parkinsonism: dystrophic changes in medium spiny neurons and progression in Parkinson's disease. J Neural Transm Suppl 67-70.

Deutch AY, Colbran RJ, Winder DJ (2007) Striatal plasticity and medium spiny neuron dendritic remodeling in parkinsonism. Parkinsonism Relat Disord 13:S251-S258.

DeVito JL, Anderson, ME (1982) An autoradiographic study of efferent connections of the globus pallidus in Macaca mulatta. Exp Brain Res 46:107-117.

DiGregorio DA, Nusser Z, Silver RA (2002) Spillover of glutamate onto synaptic AMPA receptors enhances fast transmission at a cerebellar synapse. Neuron 35:521-33.

Fan KY, Baufreton J, Surmeier DJ, Chan CS, Bevan MD (2012) Proliferation of external globus pallidus-subthalamic nucleus synapses following degeneration of midbrain dopamine neurons. J Neurosci 32:13718-13728.

Fiala JC, Spacek J, Harris KM (2002) Dendritic spine pathology: cause or consequence of neurological disorders? Brain Res Brain Res Rev 39:29-54.

Fiala JC (2005) Reconstruct: a free editor for serial section microscopy. J Microsc 218:52-61.

Fornai F, Bassi L, Bonaccorsi I, Giorgi F, Corsini GU (1997a) Noradrenaline loss selectivity exacerbates nigrostriatal toxicity in different species of rodents. Funct Neurol 12:193-198.

Fornai F, Alessandri MG, Torracca MT, Bassi L, Corsini GU (1997b) Effects of noradrenergic lesions on MPTP/MPP^+ kinetics and MPTP-induced nigrostriatal dopamine depletions. J Pharmacol Exp Ther 283:100-107.

Fornai F, di Poggio AB, Pellegrini A, Ruggieri S, Paparelli A (2007) Noradrenaline in Parkinson's disease: from disease progression to current therapeutics. Curr Med Chem 14:2330-2334.

Francois C, Percheron G, Parent A, Sadikot AF, Fenelon G, Yelnik J (1991) Topography of the projection from the central complex of the thalamus to the sensorimotor striatal territory in monkeys. J Comp Neurol 305:17-34.

Gai WP, Halliday GM, Blumbergs PC, Geffen LB, Blessing WW (1991) Substance P-containing neurons in the mesopontine tegmentum are severely affected in Parkinson's disease. Brain 114:2253-2267.

Galvan A, Hu X, Smith Y, Wichmann T (2010) Localization and function of GABA transporters in the globus pallidus of parkinsonian monkeys. Exp Neurol 223:505-15.

Galvan A, Smith Y (2011) The primate thalamostriatal system: anatomical organization, functional roles and possible involvement in Parkinson's disease. Basal Ganglia 1:179-189.

Grunwerg BS, Krauthamer GM (1992) Sensory responses of intralaminar thalamic neurons activated by the superior colliculus. Exp Brain Res 88:541-550.

Guehl D, Pessiglione M, Francois C, Yelnik J, Hirsch EC, Feger J, Tremblay L (2003) Tremor-related activity of neurons in the "motor" thalamus: changes in firing rate and pattern in the MPTP vervet model of parkinsonism. Eur J Neurosci 17:2388-2400.

Halassa MM, Acsády L (2016) Thalamic Inhibition: Diverse Sources, Diverse Scales. Trends Neurosci 39:680-693.

Halliday GM, Gai WP, Blessing WW, Geffen LB (1990) Substance P-containing neurons in the pontomesencephalic tegmentum of the human brain. Neuroscience 39:81-96.

Halliday GM (2009) Thalamic changes in Parkinson's disease. Parkinsonism Relat Dis 15:S153-S155.

Halliday G, Lees A, Stern M (2011) Milestones in Parkinson's disease-clinical and pathologic features. Mov Disord 26:1015-1021.

Hammond C, Bergman H, Brown P (2007) Pathological synchronization in Parkinson's disease: networks, models and treatments. Trends Neurosci 30:357-64.

Harris KM, Kater SB (1994) Dendritic spines: cellular specializations imparting both stability and flexibility to synaptic function. Annu Rev Neurosci 17:341-371.

Harris KM, Perry E, Bourne J, Feinberg M, Ostroff L, Hurlburt J (2006) Uniform serial sectioning for transmission electron microscopy. J Neurosci 26:12101-12103.

Heinsen H, Rub U, Gangnus D, Jungkunz G, Bauer M, Ulmar G, Bethke B, Schuler M, Bocker F, Eisenmenger W, Gotz M, Strik M (1996) Nerve cell loss in the thalamic centromedian-parafascicular complex in patients with Huntington's disease. Acta Neuropathol 91:161-168.

Henderson JM, Carpenter K, Cartwright H, Halliday GM (2000a) Loss of thalamic intralaminar nuclei in progressive supranuclear palsy and Parkinson's disease: clinical and therapeutic implications. Brain 123:1410-1421.

Henderson JM, Carpenter K, Cartwright H, Halliday GM (2000b) Degeneration of the centre median-parafascicular complex in Parkinson's disease. Ann Neurol 47:345-352.

Henderson JM, Schleimer SB, Allbutt H, Dabholkar V, Abela D, Jovic J, Quinlivan M (2005) Behavioural effects of parafascicular thalamic lesions in an animal model of parkinsonism. Behav Brain Res 162:222-232.

Hirsch EC, Graybiel AM, Duyckaerts C, Javoy-Agid F (1987) Neuronal loss in the pedunculopontine tegmental nucleus in Parkinson disease and in progressive supranuclear palsy. Proc Natl Acad Sci USA 84:5976-5980.

Hoover JE, Strick PL (1993) Multiple output channels in the basal ganglia. Science 259:819-21.

Huerta MF, Krubitzer LA, Kaas JH (1986) Frontal eye field as defined by intracortical microstimulation in squirrel monkeys, owl monkeys, and macaque monkeys: I. Subcortical connections. J Comp Neurol 253:415-439.

Hutchison WD, Lozano AM, Davis KD, Saint-Cyr JA, Lang AE, Dostrovsky JO (1994) Differential neuronal activity in segments of globus pallidus in Parkinson's disease patients. Neuroreport 5:1533-1537.

Ichinohe N, Mori F, Shoumura K (2000) A di-synaptic projection from the lateral cerebellar nucleus to the laterodorsal part of the striatum via the central lateral nucleus of the thalamus in the rat. Brain Res 880:191-197.

Ilinsky IA (1990) Structural and connectional diversity of the primate motor thalamus: experimental light and electron microscopic studies in the rhesus monkey. Stereotact Funct Neurosurg 54-55:114-24.

Ilinsky IA, Tourtellotte WG, Kultas-Ilinsky K (1993) Anatomical distinctions between the two basal ganglia afferent territories in the primate motor thalamus. Stereotact Funct Neurosurg 60:62-9.

Ilinsky IA, Yi H, Kultas-Ilinsky K (1997) Mode of termination of pallidal afferents to the thalamus: a light and electron microscopic study with anterograde tracers and immunocytochemistry in Macaca mulatta. J Comp Neurol 386:601-12.

Ingham CA, Hood SH, Arbuthnott GW (1989) Spine density on neostriatal neurones changes with 6-hydroxydopamine lesions and with age. Brain Res 503:334-338.

Ingham CA, Hood SH, Taggart P, Arbuthnott GW (1998) Plasticity of synapses in the rat neostriatum after unilateral lesion of the nigrostriatal dopaminergic pathway. J Neurosci 18:4732-4743.

Ipekchyan NM (2011) Comparative analysis of the quantitative characteristics of the corticothalamic projections of parietal cortex fields 5 and 7. Neurosci Behav Physiol 41:10-12.

Jellinger K (1988) The pedunculopontine nucleus in Parkinson's disease, progressive supranuclear palsy and Alzheimer's disease. J Neurol Neurosurg Psychiatry 51:540-543.

Jones EG (2007) The Thalamus, Vol. 1 and 2, Cambridge University Press, New York.

Kammermeier S, Pittard D, Hamada I, Wichmann T (2016) Effects of high-frequency stimulation of the internal pallidal segment on neuronal activity in the thalamus in parkinsonian monkeys. J Neurophysiol 116:2869-2881.

Kliem MA, Wichmann T (2004) A method to record changes in local neuronal discharge in response to infusion of small drug quantities in awake monkeys. J Neurosci Methods 138:45-9.

Kliem MA, Maidment NT, Ackerson LC, Chen S, Smith Y, Wichmann T (2007) Activation of nigral and pallidal dopamine D1-like receptors modulates basal ganglia outflow in monkeys. J Neurophysiol 98:1489-1500.

Knott G, Marchman H, Wall D, Lich B (2008) Serial section scanning electron microscopy of adult brain tissue using focused ion beam milling. J Neurosci 28:2959-2964.

Kultas-Ilinsky K, Ilinsky IA (1990) Fine structure of the magnocellular subdivision of the ventral anterior thalamic nucleus (VAmc) of *Macaca mulatta*: II. Organization of nigrothalamic afferents as revealed with EM autoradiography. J Comp Neurol 294:479-489.

Kultas-Ilinsky K, Reising L, Yi H, Ilinsky IA (1997) Pallidal afferent territory of the Macaca mulatta thalamus: neuronal and synaptic organization of the VAdc. J Comp Neurol 386:573-600.

Kunzle H (1976) Thalamic projections from the precentral motor cortex in Macaca fascicularis. Brain Res 105:253-267.

Kunzle H (1978) An autoradiographic analysis of the efferent connections from premotor and adjacent prefrontal regions (areas 6 and 9) in macaca fascicularis. Brain Behav Evol 15:185-234.

Kuroda M, Price JL (1991) Ultrastructure and synaptic organization of axon terminals from brainstem structures to the mediodorsal thalamic nucleus of the rat. J Comp Neurol 313:539-552.

Kuwajima M, Spacek J, Harris KM (2012) Beyond counts and shapes: studying pathology of dendritic spines in the context of the surrounding neuropil through serial section electron microscopy. Neuroscience 251:75-89.

Kuypers HG, Lawrence DG (1967) Cortical projections to the red nucleus and the brain stem in the Rhesus monkey. Brain Res 4:151-188.

Lacey CJ, Bolam JP, Magill PJ (2007) Novel and distinct operational principles of intralaminar thalamic neurons and their striatal projections. J Neurosci 27:4374-4384.

Lavallée P, Urbain N, Dufresne C, Bokor H, Acsády L, Deschênes M (2005) Feedforward inhibitory control of sensory information in higher-order thalamic nuclei. J Neurosci 25:7489-98.

Leichnetz GR, Goldberg ME (1988) Higher centers concerned with eye movement and visual attention: cerebral cortex and thalamus. Rev Oculomot Res 2:365-429.

Magnin M, Morel A, Jeanmonod D (2000) Single-unit analysis of the pallidum, thalamus and subthalamic nucleus in parkinsonian patients. Neuroscience 96:549-64.

Marien M, Briley M, Colpaert F (1993) Noradrenaline depletion exacerbates MPTP-induced striatal dopamine loss in mice. Eur J Pharmacol 236:487-489.

Masilamoni G, Votaw J, Howell L, Villalba RM, Goodman M, Voll RJ, Stehouwer J, Wichmann T, Smith Y (2010) (18)F-FECNT: validation as PET dopamine transporter ligand in parkinsonism. Exp Neurol 226:265-273.

Masilamoni GJ, Bogenpohl JW, Alagille D, Delevich K, Tamagnan G, Votaw JR, Wichmann T, Smith Y (2011) Metabotropic glutamate receptor 5 antagonist protects dopaminergic and noradrenergic neurons from degeneration in MPTP-treated monkeys. Brain 134:2057-2073.

Mathai A, Ma Y, Paré JF, Villalba RM, Wichmann T, Smith Y (2015) Reduced cortical innervation of the subthalamic nucleus in MPTP-treated parkinsonian monkeys. Brain 138:946-62.

McFarland NR, Haber SN (2000) Convergent inputs from thalamic motor nuclei and frontal cortical areas to the dorsal striatum in the primate. J Neurosci 20:3798-3813.

McFarland NR, Haber SN (2001) Organization of thalamostriatal terminals from the ventral motor nuclei in the macaque. J Comp Neurol 429:321-336.

Mitchell IJ, Clarke CE, Boyce S, Robertson RG, Peggs D, Sambrook MA, et al. (1989) Neural mechanisms underlying parkinsonian symptoms based upon regional uptake of 2-deoxyglucose in monkeys exposed to 1-methyl-4-phenyl-1,2,3,6-tetrahydropyridine. Neuroscience 32:213-226.

Molnar GF, Pilliar A, Lozano AM, Dostrovsky JO (2005) Differences in neuronal firing rates in pallidal and cerebellar receiving areas of thalamus in patients with Parkinson's disease, essential tremor, and pain. J Neurophysiol 93:3094-101.

Ni ZG, Gao DM, Benabid AL, Benazzouz A (2000) Unilateral lesion of the nigrostriatal pathway induces a transient decrease of firing rate with no change in the firing pattern of neurons of the parafascicular nucleus in the rat. Neuroscience 101:993-999.

Parent A, Hazrati LN (1995) Functional anatomy of the basal ganglia. I. The cortico-basal ganglia-thalamo-cortical loop. Brain Res Rev 20:91-127.

Parent M, Parent A (2005) Single-axon tracing and three-dimensional reconstruction of centre median-parafascicular thalamic neurons in primates. J Comp Neurol 481:127-144.

Pessiglione M, Guehl D, Rolland AS, François C, Hirsch EC, Féger J, Tremblay L (2005) Thalamic neuronal activity in dopamine-depleted primates: evidence for a loss of functional segregation within basal ganglia circuits. J Neurosci 25:1523-1531.

Raju DV, Shah DJ, Wright TM, Hall RA, Smith Y (2006) Differential synaptology of vGluT2-containing thalamostriatal afferents between the patch and matrix compartments in rats. J Comp Neurol 499:231-243.

Raju DV, Ahern TH, Shah DJ, Wright TM, Standaert DG, Hall RA, Smith Y (2008) Differential synaptic plasticity of the corticostriatal and thalamostriatal systems in an MPTP-treated monkey model of parkinsonism. Eur J Neurosci 27:1647-1658.

Redgrave P, Rodriguez M, Smith Y, Rodriguez-Oroz MC, Lehericy S, Bergman H, Agid Y, DeLong MR, Obeso JA (2010) Goal-directed and habitual control in the basal ganglia: implications for Parkinson's disease. Nat Rev Neurosci 11:760-772.

Rolland AS, Herrero MT, Garcia-Martinez V, Ruberg M, Hirsch EC, François C (2007) Metabolic activity of cerebellar and basal ganglia-thalamic neurons is reduced in Parkinsonism. Brain 130:265-275.

Rommelfanger KS, Weinshenker D (2007) Norepinephrine: the redheaded stepchild of Parkinson's disease. Biochem Pharmacol 74:177-190.

Rommelfanger KS, Edwards GL, Freeman KG, Liles LC, Miller GW, Weinshenker D (2007) Norepinephrine loss produces more profound motor deficits than MPTP treatment in mice. Proc Natl Acad Sci USA 104:13804-13809.

Rovó Z, Ulbert I, Acsády L (2012) Drivers of the primate thalamus. J Neurosci 32:17894-908.

Royce GJ, Bromley S, Gracco C (1991) Subcortical projections to the centromedian and parafascicular thalamic nuclei in the cat. J Comp Neurol 306:129-155.

Sadikot AF, Parent A, Francois C (1992a) Efferent connections of the centromedian and parafascicular thalamic nuclei in the squirrel monkey: a PHA-L study of subcortical projections. J Comp Neurol 315:137-159.

Sadikot AF, Parent A, Smith Y, Bolam JP (1992b) Efferent connections of the centromedian and parafascicular thalamic nuclei in the squirrel monkey: a light and electron microscopic study of the thalamostriatal projection in relation to striatal heterogeneity. J Comp Neurol 320:228-242.

Sakai ST, Grofova I, Bruce K (1998) Nigrothalamic projections and nigrothalamocortical pathway to the medial agranular cortex in the rat: single- and double-labeling light and electron microscopic studies. J Comp Neurol 391:506-525.

Sidibe M, Bevan MD, Bolam JP, Smith Y (1997) Efferent connections of the internal globus pallidus in the squirrel monkey: I. Topography and synaptic organization of the pallidothalamic projection. J Comp Neurol 382:323-347.

Sidibe M, Pare JF, Smith Y (2002) Nigral and pallidal inputs to functionally segregated thalamostriatal neurons in the centromedian/parafascicular intralaminar nuclear complex in monkey. J Comp Neurol 447:286-99.

Smith Y, Parent A (1986) Differential connections of caudate nucleus and putamen in the squirrel monkey (Saimiri sciureus) Neuroscience 18:347-371.

Smith Y, Sidibe, M (2003) The Thalamus. In: Neuroscience in Medicine. Vol., P.M. Conn, ed. eds. Humana Press Inc., Totowa, NJ.

Smith Y, Raju DV, Pare JF, Sidibe M (2004) The thalamostriatal system: a highly specific network of the basal ganglia circuitry. Trends Neurosci 27:520-527.

Smith Y, Raju D, Nanda B, Pare JF, Galvan A, Wichmann T (2009) The thalamostriatal systems: anatomical and functional organization in normal and parkinsonian states. Brain Res Bull 78:60-68.

Smith Y, Galvan A, Raju D, Wichmann T (2010) “Anatomical and functional organization of the thalamostriatal systems,” in Handbook of Basal Ganglia Structure and Function: A Decade of Progress, eds. H. Steiner and K. Y. Tseng (New York, NY: Elsevier), 381–392.

Smith Y, Surmeier DJ, Redgrave P, Kimura M (2011) Thalamic contributions to Basal Ganglia-related behavioral switching and reinforcement. J Neurosci.31:16102-16106.

Soares J, Kliem MA, Betarbet R, Greenamyre JT, Yamamoto B, Wichmann T (2004) Role of external pallidal segment in primate parkinsonism: comparison of the effects of 1-methyl-4-phenyl-1,2,3,6-tetrahydropyridine-induced parkinsonism and lesions of the external pallidal segment. J Neurosci 24:6417-6426.

Stephens B, Mueller AJ, Shering AF, Hood SH, Taggart P, Arbuthnott GW, Bell JE, Kilford L, Kingsbury AE, Daniel SE, Ingham CA (2005) Evidence of a breakdown of corticostriatal connections in Parkinson's disease. Neuroscience 132:741-754.

Suarez LM, Solis O, Aguado C, Lujan R, Moratalla R (2016) L-DOPA oppositely regulates synaptic strength and spine morphology in D1 and D2 striatal projection neurons in dyskinesia. Cereb Cortex 26:4253-4264.

Swain AJ, Kelly H, Pare JF, Galvan A, Wichmann T, Smith Y (2017) Structural Plasticity of GABAergic and Glutamatergic inputs to the Ventral Motor and Caudal Intralaminar Thalamic Nuclei in MPTP-treated Parkinsonian Monkeys. Society for Neuroscience Abstracts

Swain AJ, Kelly H, Smith Y (2018) Ultrastructural features of single pallidothalamic terminals in control and MPTP-treated Parkinsonian monkeys visualized using 3D electron microscopic reconstruction approaches. Society for Neuroscience Abstracts

Telgkamp P, Padgett DE, Ledoux VA, Woolley CS, Raman IM (2004) Maintenance of high-frequency transmission at purkinje to cerebellar nuclear synapses by spillover from boutons with multiple release sites. Neuron 41:113-126.

Tsumori T, Yokota S, Ono K, Yasui Y (2002) Synaptic organization of GABAergic projections from the substantia nigra pars reticulata and the reticular thalamic nucleus to the parafascicular thalamic nucleus in the rat. Brain Res 957:231-241.

Villalba RM, Lee H, Smith Y (2009) Dopaminergic denervation and spine loss in the striatum of MPTP-treated monkeys. Exp Neurol 215:220-227.

Villalba RM, Smith Y (2010) Striatal spine plasticity in Parkinson's disease. Front Neuroanat 4:133.

Villalba, RM, Smith Y (2011a) Differential structural plasticity of corticostriatal and thalamostriatal axo-spinous synapses in MPTP-treated Parkinsonian monkeys. J Comp Neurol 519:989-1005.

Villalba RM, Smith Y (2011b) Neuroglial plasticity at striatal glutamatergic synapses in Parkinson's disease. Front Syst Neurosci 5:68.

Villalba RM, Smith Y (2013) Differential striatal spine pathology in Parkinson's disease and cocaine addiction: a key role of dopamine? Neuroscience 251:2-20.

Villalba RM, Wichmann T, Smith Y (2014) Neuronal loss in the caudal intralaminar thalamic nuclei in a primate model of Parkinson's disease. Brain Struct Funct 219:381-394.

Villalba RM, Mathai A, Smith Y (2015) Morphological changes of glutamatergic synapses in animal models of Parkinson's disease. Front Neuroanat 9:117.

Villalba RM, Smith Y (2018) Loss and remodeling of striatal dendritic spines in Parkinson's disease: from homeostasis to maladaptive plasticity?. J Neural Transm 125:431-447.

Vitek JL, Ashe J, Kaneoke Y (1994) Spontaneous neuronal activity in the motor thalamus: alteration in pattern and rate in parkinsonism. Society for Neuroscience Abstracts 20:561.

Wanaverbecq N, Bodor ÁL, Bokor H, Slézia A, Lüthi A, Acsády L (2008) Contrasting the functional properties of GABAergic axon terminals with single and multiple synapses in the thalamus. J Neurosci 28:11848-11861.

Wichmann T, DeLong MR (1996) Functional and pathophysiological models of the basal ganglia. Curr Opin Neurobiol 6:751-8.

Wichmann T, Bergman H, Starr PA, Subramanian T, Watts RL, DeLong MR (1999) Comparison of MPTP-induced changes in spontaneous neuronal discharge in the internal pallidal segment and in the substantia nigra pars reticulata in primates. Exp Brain Res 125:397-409.

Wichmann T, Kliem MA, DeLong MR (2001) Antiparkinsonian and behavioral effects of inactivation of the substantia nigra pars reticulata in hemiparkinsonian primates. Exp Neurol 167:410-424.

Wichmann T, DeLong MR (2003) Pathophysiology of Parkinson's disease: the MPTP primate model of the human disorder. Ann N Y Acad Sci 991:199-213.

Wichmann T, Soares J (2006) Neuronal firing before and after burst discharges in the monkey basal ganglia is predictably patterned in the normal state and altered in parkinsonism. J Neurophysiol 95:2120-33.

Wichmann T, Delong MR (2007) Anatomy and physiology of the basal ganglia: relevance to Parkinson’s disease and related disorders. Handb Clin Neurol 83:1-18.

Williams-Gray CH, Foltynie T, Lewis SJ, Barker RA (2006) Cognitive deficits and psychosis in Parkinson's disease: a review of pathophysiology and therapeutic options. CNS Drugs 20:477-505.

Xu-Friedman, MA, Regehr WG (2004) Structural contributions to short-term synaptic plasticity. Physiol. Rev 84:69-85.

Xuereb JH, Perry RH, Candy JM, Perry EK, Marshall E, Bonham JR (1991) Nerve cell loss in the thalamus in Alzheimer's disease and Parkinson's disease. Brain 114:1363-1379.

Yuste R, Bonhoeffer T (2001) Morphological changes in dendritic spines associated with long-term synaptic plasticity. Annu Rev Neurosci 24:1071-1089.

Zaja-Milatovic S, Milatovic D, Schantz AM, Zhang J, Montine KS, Samii A, Deutch AY, Montine TJ (2005) Dendritic degeneration in neostriatal medium spiny neurons in Parkinson disease. Neurology 64:545-547.

Zirh TA, Lenz FA, Reich SG, Dougherty PM (1998) Patterns of bursting occurring in thalamic cells during parkinsonian tremor. Neuroscience 83:107-121.

Zucker RS, Regehr WG (2002) Short-term synaptic plasticity. Annu Rev Physiol 64:355-405.